Swiss J Geosci (2016) 109:37–56
DOI 10.1007/s00015-016-0206-7

Formation of an intra-orogenic transtensional basin: the Neogene Wagrain basin in the Eastern Alps

Franz Neubauer[1]

Received: 23 June 2015 / Accepted: 7 January 2016 / Published online: 11 February 2016

Abstract The Neogene (ca. Ottnangian to Lower Badenian) Wagrain basin formed within a halfgraben, close to the north-eastern edge of the exhuming and uplifting Neogene Tauern metamorphic core complex, along the ENE-trending, ca. orogen-parallel sinistral-transtensional Salzach-Enns and Mandling fault systems of the Eastern Alps. Based on a pronounced colour change from thin basal reddish, hematite-rich conglomerates to grey-brownish clastics, the basin infill records a climate change from a subtropical to a humid temperate climate. The change is used as a proxy for the dating of the basin as a similar regional climate shift has been reported, e.g., from other fault-bounded basins in the Eastern Alps and from the base Styrian basin predating there Ottnangian coal-bearing deposits. The lithofacies evolution of the Wagrain basin fill shows initial rapid subsidence and infilling by fluvial, massive, coarse-grained conglomerates and subsequent mica-rich immature sandstones deposited in a prodelta environment of a lake. The conglomerates were mainly shed from a polymetamorphic, medium-grade metamorphic basement similar to the Austroalpine Altkristallin basement complex, which is not exposed in the present surroundings of the basin. Provenance studies particularly suggest the Schladming/Bösenstein and Wölz Micaschist complexes as possible sources. The sandstones are extremely rich in mica, similar to ones found in many late-stage orogenic sandstones of other orogens, and garnet. Provenance analysis contrasts recent models for the Neogene evolution of the Eastern Alps, which assume a phyllitic source for similar conglomerates exposed further north and northeast. Fault and striae of the Wagrain basin fill allow deduce two post-depositional palaeostress tensor orientations: WNW-ESE extension and ca. E-W contraction. This data is consistent with palaeostress development along the Salzach-Enns fault, which also confines the Tauern metamorphic core complex, and shows an evolution from sinistral transtensional to sinistral transpressional to post-depositional dextral transpression.

Keywords Orogenic collapse · Provenance analysis · Halfgraben · Transtension · Ar–Ar dating · Sandstone composition

1 Introduction

Many models have been developed to explain the formation of intramontane, often small-scaled terrestrial sedimentary basins during late orogenic stages within mountain belts (Seguret et al. 1989). A general feature is the linkage with major regional, often orogeny-parallel strike-slip faults (e.g., Sylvester 1988; Ratschbacher et al. 1989, 1991; Allen and Allen 1990; Einsele 1992; Leeder 1999; Cunningham and Mann 2007). These basins form during surface uplift and also due to (?) updoming and exhumation of previously deeply buried metamorphic core complexes in central zones of the orogen. The basin fill monitors, therefore, the increasing relief and its erosion.

In this respect, the Neogene fault pattern of the Eastern Alps is of special interest because of its interpretation as a set of conjugate strike-slip faults (Buchroithner 1984), which led to the extrusion/escape of an intra-orogenic

Editorial handling: W. Winkler.

✉ Franz Neubauer
franz.neubauer@sbg.ac.at

[1] Department Geography and Geology, University of Salzburg, Hellbrunner Straße 34, 5020 Salzburg, Austria

block from the Eastern Alps towards the Carpathians (Fig. 1; Neubauer 1988; Ratschbacher et al. 1989, 1991; Neubauer and Genser 1990; Peresson and Decker 1997a, b; Frisch et al. 1998). These fault systems include the sinistral Salzach-Enns and Mur-Mürz fault systems in the northern part and the dextral Periadriatic fault system in the south (Fig. 1). Many small Neogene basins have been explained as pull-apart and transcurrent basins owing to basin geometry and relationships to major fault zones related to the sinistral Salzach-Enns and Mur-Mürz fault systems (Nievoll 1985; Royden 1985; Tollmann 1985; Neubauer 1988; Ratschbacher et al. 1991; Zeilinger et al. 1999; Eder and Neubauer 2000; Neubauer et al. 2000; Sachsenhofer et al. 2000; Strauss et al., 2001; Neubauer and Unzog 2003). Among these, the large Vienna basin is interpreted to represent a large pull-apart basin (Royden 1985; Wessely 1988; Fodor 1995). In contrast, the contemporaneously formed Styrian and the easterly adjacent Pannonian basins are explained to result from E–W extension (e.g. Royden 1988; Bergerat 1989; Ratschbacher et al. 1989, 1991; Neubauer and Genser 1990; Friebe 1991; Sachsenhofer et al. 1997; Fodor et al. 1999) and represents, therefore, a collapse basin on top of the collapsing Alpine orogenic wedge. The Waldheimat basin (Fig. 1) is interpreted to have formed by ca. N–S transtension during east-directed lateral extrusion (Neubauer and Unzog 2003).

During recent years, a lot of original, new data on and models the Oligocene to Neogene near-surface and geomorphologic evolution of the Eastern Alps have been presented (e.g., Frisch et al. 1998, 2000a; Kuhlemann et al. 2001a, b; Robl et al. 2008a, b). They found a significant difference between the eastern part of the Eastern Alps with sedimentation of the coarse clastics of the Augenstein Formation with a supposed Oligocene/Early Neogene age and the western part, where, except for the Inntal basin (Fig. 1; Ortner and Stingl 2001), no Oligocene to Neogene sedimentary basins were found. The overall partition line was at ca. the meridian of the northeastern edge of the Tauern window (Frisch et al. 2001). They assumed that the present surface of western sectors of the Eastern Alps was

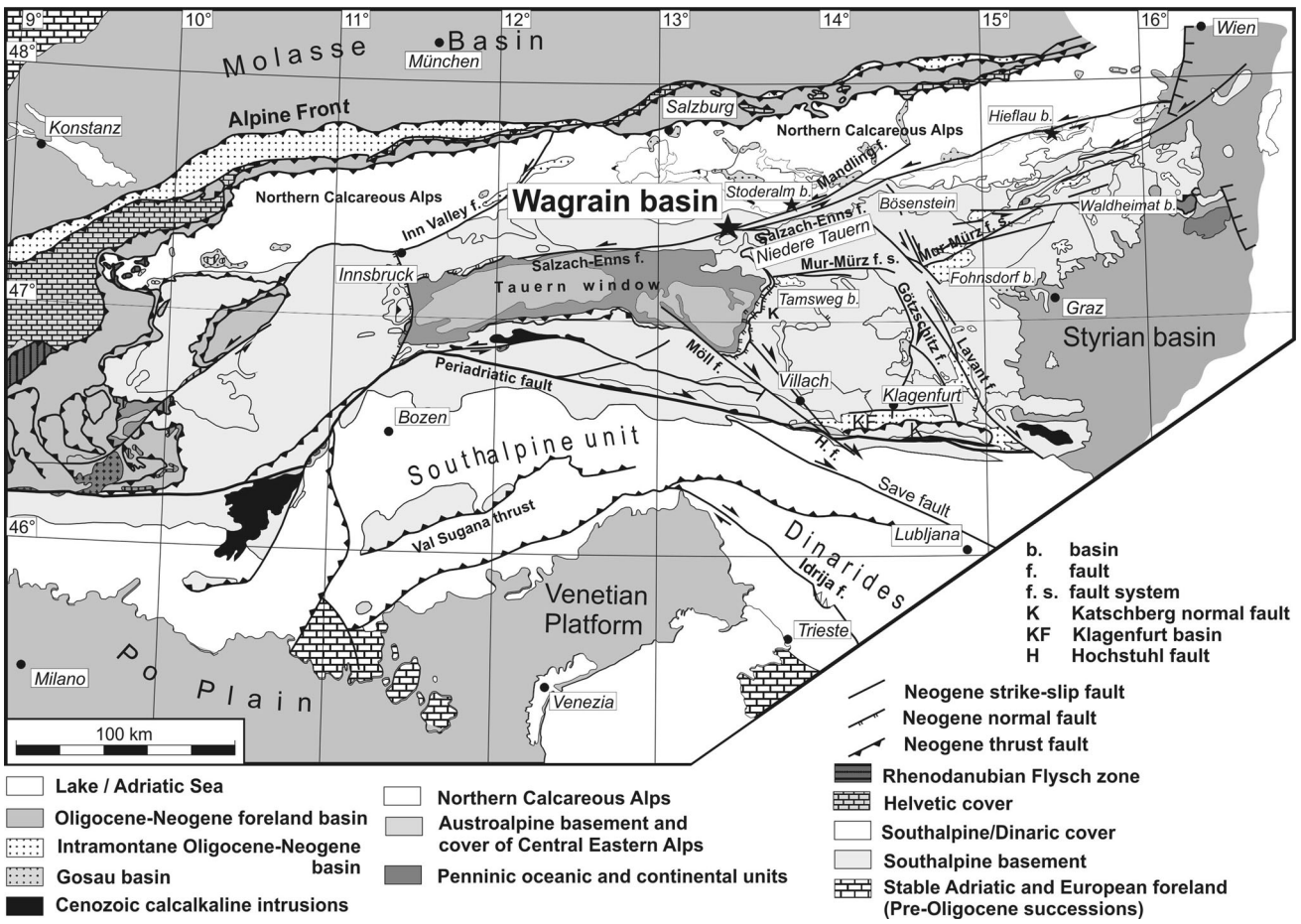

Fig. 1 Neogene fault pattern in the Eastern Alps (modified after Neubauer et al. 2000). Note the ca. eastward motion of the Neogene extruding wedge. The extrusion wedge is confined by the dextral Periadriatic fault and the sinistral Salzach-Enns- (earlier) and Mur-Mürz (later) wrench corridors. Note also the exhumed Tauern metamorphic core complex (Tauern window in the figure)

still deeply buried in Oligocene and Early Miocene times, and that rocks were exhumed there no earlier than Early/Middle Miocene (Frisch et al. 1998, 2000a). The Wagrain basin is of special interest because its location close to the Tauern metamorphic core complex, which was exhumed and uplifted during the same time as the basin formed (Sachsenhofer 1988; Neubauer et al. 1999; Liu et al. 2001; Frisch et al. 2000b). The Salzach-Enns fault, confining both the Tauern window and the Wagrain basin, is considered to represent the master fault governing the basin subsidence (e.g. Wang and Neubauer 1998).

Here, we present an integrated study covering structure, sedimentology, provenance and fault orientations to constrain the evolution of the small, but well-exposed, fault-bounded Wagrain basin (Petrascheck 1924, 1937; Trauth 1925; Weber and Weiss 1983; Exner 1996). It formed along the dextral ENE-trending Mandling fault and close to the northern, sinistral confining Salzach-Enns fault, which also guided the exposure of the Tauern metamorphic core complex. No modern study is available, which shows the relationship of basin formation, sedimentological and structural evolution and the linkage of basin formation with exhumation of the Tauern metamorphic core complex (Scharf et al. 2013 and references therein).

The Paratethys time-scale calibration and chronostratigraphy used in this paper is that of Piller et al. (2007).

2 Geological setting

The Wagrain basin is an intramontane Neogene basin located adjacent to low-grade metamorphic Lower Palaeozoic basement rocks (Wagrain Phyllite; Schönlaub, 1979) of the Lower Austroalpine nappe complex of the Radstadt Mountains close to the north-eastern edge of the Tauern metamorphic core complex (Fig. 2). This basin is one of a few isolated Neogene basins considered to be located along the Salzach-Enns fault (e.g., Winkler 1928; Tollmann 1985; Ratschbacher et al. 1991; Peresson and Decker 1997a, b; Keil and Neubauer 2009; Figs. 1, 2). The Salzach-Enns fault is a sinistral transtensive fault, along which the southern block was exhumed (Genser and Neubauer 1989; Ratschbacher et al. 1991; Wang and Neubauer 1998; Frost et al. 2011).

The tectonic position of the Wagrain basin is more complicated than previously considered and is described here in N–S cross-section. As it is already obvious from detailed mapping by Exner (1996), the easternmost portion of the basin is exposed to the north of the Mandling wedge (Hirschberg 1965). The Mandling wedge is a fault-bounded block composed mainly of Middle and Upper Triassic dolomitic cover rocks originating from the Northern Calcareous Alps (Upper Austroalpine nappe complex). The Mandling wedge widens to the east and is exposed between the Mandling fault/North Enns Valley fault (Keil and Neubauer 2011) in the north and the Salzach-Enns fault in the south (Fig. 2). At Wagrain, small lenses of a reddish slate and metasandstone likely of Permian age may represent the western most outlier of the Mandling wedge (Fig. 3 for location). The Wagrain basin is therefore not strictly located along the Salzach-Enns fault itself, but to the north of the merging Mandling and Salzach-Enns faults (Figs. 2, 3). The Wagrain basin fill overlies Lower Palaeozoic phyllites of the Grauwacken zone (Exner 1996 and references therein), which represents the basement of the Upper Austroalpine nappe complex.

Previous authors noted the special clast composition of the Wagrain basin fill with the dominance of gneisses similar to amphibolite-grade Middle Austroalpine basement rocks ("Altkristallin"), which are not exposed in the present surroundings of the basin (Exner 1996). This is seemingly in contrast to the Augenstein Formation of other places, which is rich in vein quartz and for which a phyllitic source is assumed (Frisch et al. 2001). No Penninic clasts have been found in the Wagrain basin. Sachsenhofer (1988) noted the high value of vitrinite reflectance due to high coalification suggesting an original thickness of ca. 1000 m of the Wagrain basin fill. The vitrinite reflectance of Neogene coals along the Enns valley increases from east to west along the Enns valley and was estimated to have reached a temperature of ca. 120 °C in the westernmost Wagrain basin and 50–80 °C in the east. The high heat flow was considered to result from waning stages of the late Alpine metamorphism in the Penninic Tauern window (Sachsenhofer 1988). Based on previously reported plant fossils, Steininger et al. (1988) proposed a Karpatian to Early Badenian age of the Wagrain basin. Dunkl et al. (2005) provided a fission track age of detrital apatite grains and found a central age of 50.0 ± 2.6 Ma excluding heating above the annealing temperature of apatite (ca. 80 °C). Márton et al. (2000) noted a ca. 15 degrees counter-clockwise rotation since the formation of the Wagrain basin. Coal exploration took place during the Second World War, and a N–S gallery penetrating the whole basin fill and the Salzach-Enns fault was built S of Steinbach (Heissel 1951; Weber and Weiss 1983).

In contrast to other regions along the strike, in the area N of the Wagrain basin, the Grauwacken zone dips to the S respectively SSW. This suggests an antiformal geometry of the Grauwacken zone (Fig. 4, section A–A′). In the Grauwacken zone and in the overlying Permian to Lower Triassic base of the Northern Calcareous Alps, fine-grained phyllitic lithologies dominate, and sericite reaches a grain size of ca. 0.1 mm. The metamorphic overprint there lies within greenschist facies conditions. Frank and Schlager (2006) reported Ar–Ar ages of very fine-grained sericite

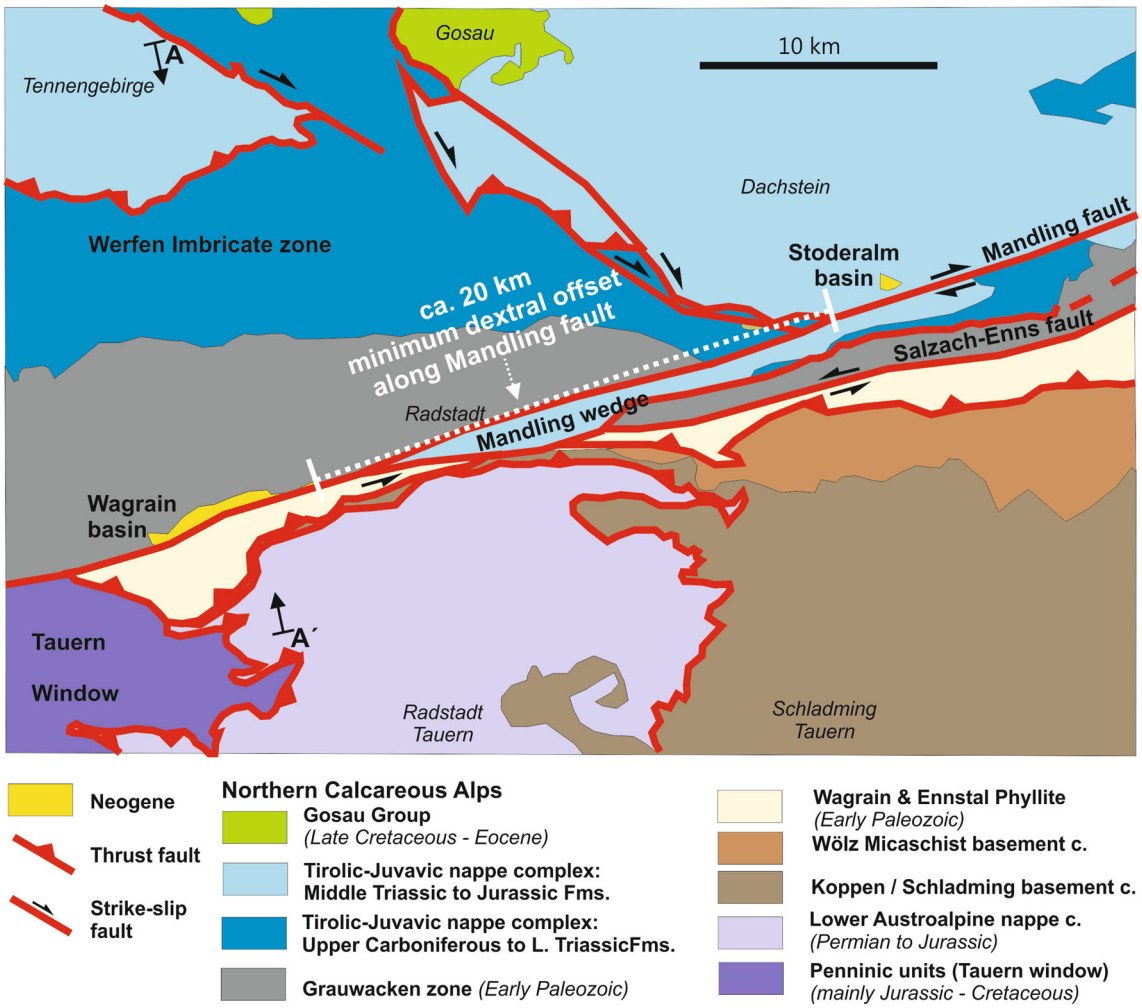

Fig. 2 Simplified geological map of the northeastern edge of the Tauern metamorphic core complex. For location, see Fig. 1. The Mandling wedge is considered to represent a dextral strike-slip duplex of the Northern Calcareous Alps. *A*–*A*′ locates section shown in Fig. 4

(ca. 30 µm) from the base of Northern Calcareous Alps to vary between 102 and 110 Ma, Schmidlechner et al. (2006) reported Ar–Ar ages of 99–102 Ma from the Grauwacken zone in the north of the Wagrain basin. To the south of the Salzach-Enns fault, the N-dipping Lower Palaeozoic Wagrain Quartzphyllite unit (Schönlaub 1975, 1979) is exposed, which merges to the east with the Ennstal Phyllite. These are underlain by retrogressed medium-grade metamorphic units, the Koppen lamella (Exner 1996), which is mainly composed of paragneiss and retrogressed amphibolite. To the east this unit merges with the Schladming complex, which comprises orthogneiss, paragneiss and amphibolite and is overlain, further east, by the Wölz Micaschist complex (Mandl et al. 2014). Cretaceous K–Ar and Rb–Sr white mica ages were reported from the Schladming and Wölz Micaschist complex (Hejl 1984; Hejl et al. 1987; Abart and Martinelli 1988; Mandl et al. 2014 and references therein). The Koppen lamella is underlain by the Lower Austroalpine Radstadt nappe complex. The Radstadt nappe complex comprises thick low-grade metamorphic Permian Alpine Verrucano-type quartz-phyllites, Lower Triassic quartzites and Middle to Upper Triassic carbonates (dolomites and banded marbles). Liu et al. (2001 and own unpublished data) dated the age of the low-grade metamorphic overprint of the Radstadt nappe complex and found an age of 78–80 Ma for the growth of sericite.

3 Basin geometry

The Wagrain basin fill was deposited onto the low-grade metamorphic, phyllitic basement of the Grauwacken zone, which dips to the south in the region. During 2004, a small exposure was found, where basal red conglomerates overly the Grauwacken zone phyllite on the western edge of the

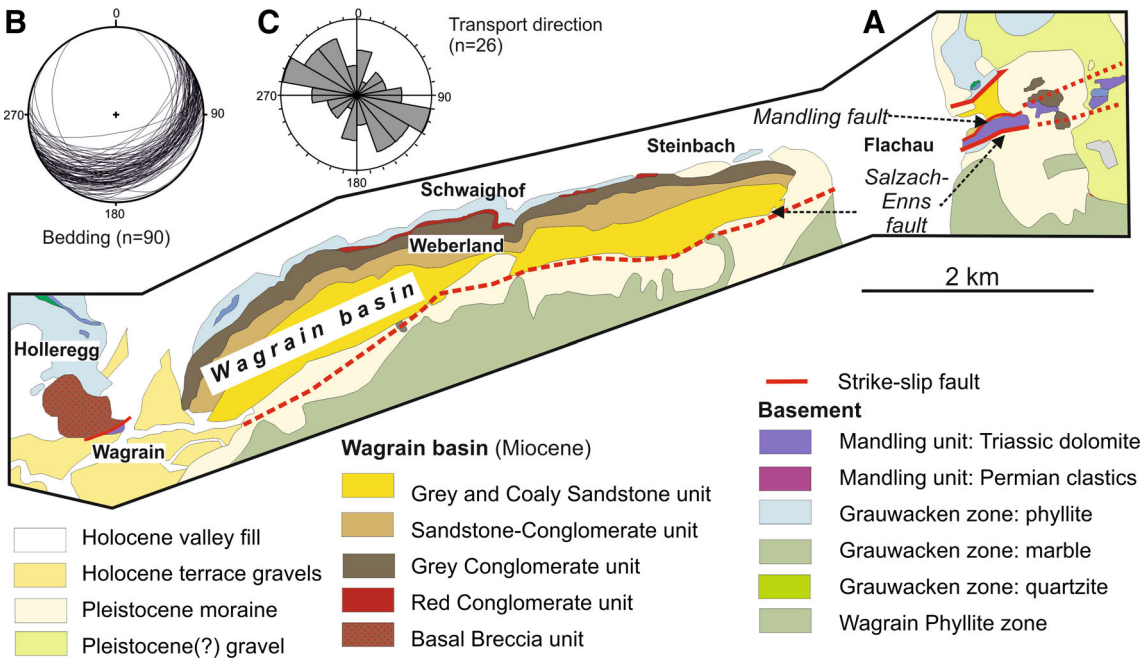

Fig. 3 **a** Geological map of the Wagrain basin. **b** Bedding planes of the Wagrain basin fill in the Schmidt projection, lower hemisphere. **c** Transport direction

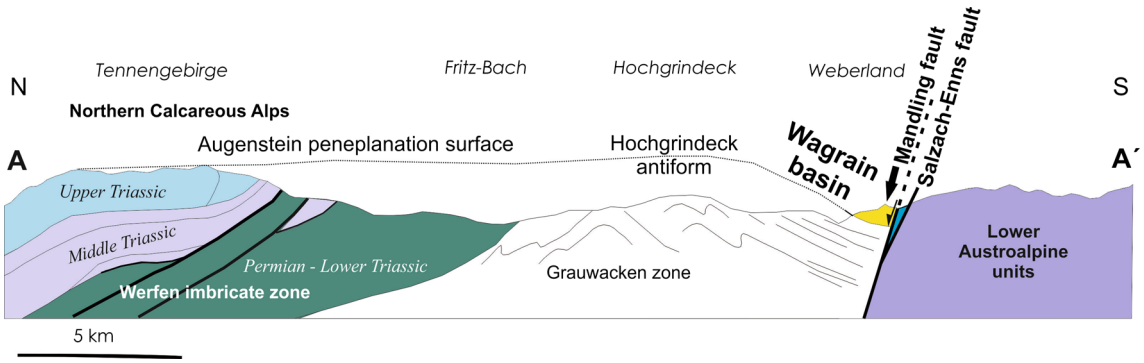

Fig. 4 Geological N–S section across the Wagrain basin. For location, see Fig. 2

entrance of the Steinbach valley (Fig. 5b). A similar observation was made by Exner (1996), who found indications for an angular unconformity near Schwaighof (for location, see Fig. 3a).

The basin itself trends ENE and is exposed over ca. 15 km from Holleregg N of Wagrain over Flachau to the north-facing slope east of Radstadt (Fig. 2). The width of the preserved basin fill is ca. 0.5–1.5 km. In western sectors, the exposure is unusually good as several deeply incised gorges cross the uplifted basin fill. The basin-fill dips gently to the SSE (Fig. 3b) and a fault contact to the Mandling wedge must be assumed. A dark fault gouge is exposed in a few localities at the boundary. Little remnants of similar Cenozoic sedimentary rocks are exposed ca. 900 m east of Radstadt as shear lenses within the Mandling fault (Trauth 1918, 1927). These were originally described as Eocene rocks and Tollmann (1985), Steininger et al. (1988) and Sachsenhofer (1988) assigned them to an extension of the Miocene Wagrain basin fill. At the northeastern extension of the same fault, the Stoderalm Neogene rocks are exposed (Fig. 2) suggesting that the Wagrain basin fill, Radstadt Neogene and Stoderalm Neogene potentially represents the infill of the same, now dismembered basin.

The overall thickness of the Wagrain at present exposed basin fill is estimated to be ca. 250–300 m in a N–S section (Figs. 5, 6). To the east, Quaternary glacial cover and Holocene valley fill veil much of the Wagrain basin. The overall, south-dipping structure, the discordant fault contact to the steeply N-dipping Mandling and Salzach-Enns

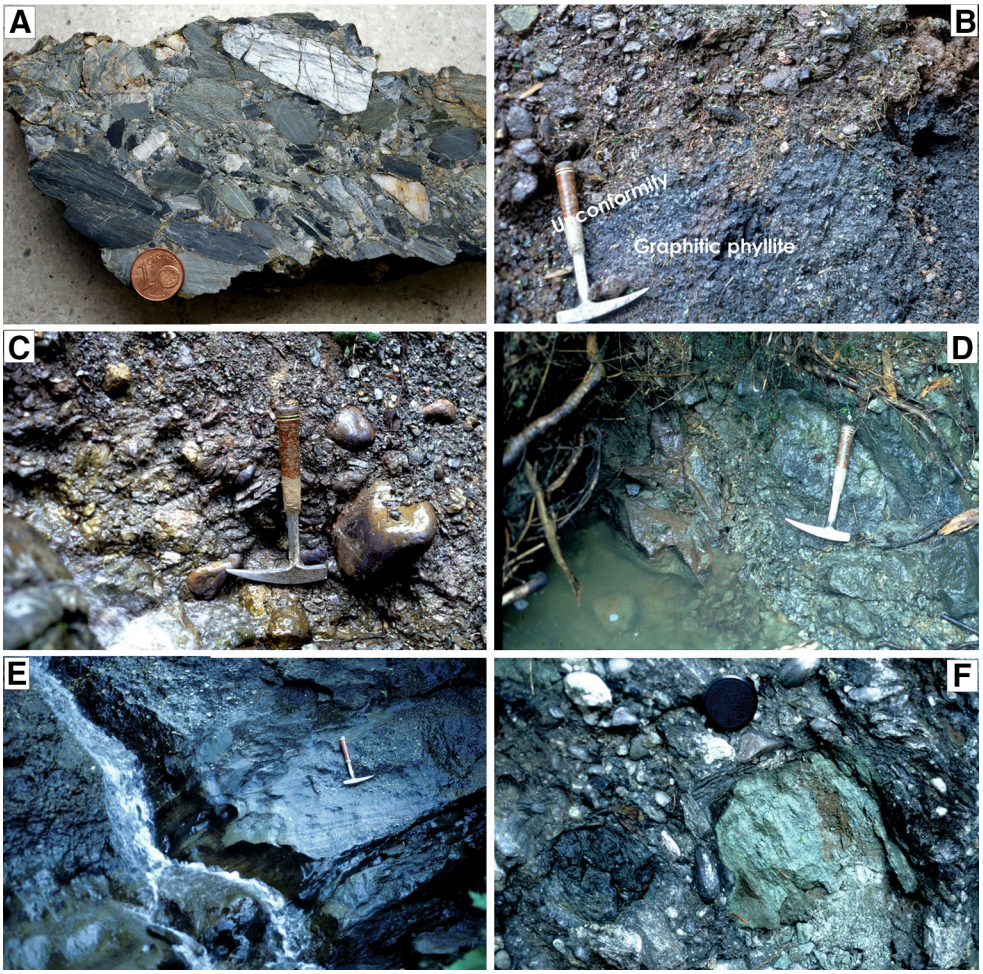

Fig. 5 Examples of lithofacies. **a** Basal Breccia unit with subangular, imbricated low-grade metamorphic clasts. **b** Basal contact of *red* conglomerates overlying *black* phyllites of the Grauwacken zone. **c** Hematite-bearing *red* conglomerate. **d** Thin breccia with large angular micaschist boulders. **e** Conglomerate/sandstone unit. Scour infill within the sandstone. **f** Coarse-grained *grey-brown* conglomerate with a large variety of metamorphic clasts

faults indicate a halfgraben structure (Fig. 3). This is supported by the antiformal structure of the Grauwacken zone in the north of the Wagrain basin, which can be interpreted as a rollover structure. The overall geometry suggests, therefore, a N–S transtensional, dextral offset along the ENE-trending Mandling fault.

4 Basin fill

The basin fill is well exposed to the north of the present-day traces of the Mandling and Salzach-Enns fault systems. Here, we introduce a number of informal mappable lithostratigraphic units, which represent distinct lithofacies and which have conformable contacts to each other. These are shown as units in the map of the Wagrain basin fill (Fig. 3). Considering all available information, the following lithofacies types can be distinguished, which follow in a vertical, respectively lateral ca. ENE-trending section. These include (Figs. 5, 6):

1. Breccia lithofacies: A breccia lithofacies (Fig. 5a) occurs only in the Holleregg area N of Wagrain (Fig. 3a) and in a few metre-scaled lenses further to the east (Fig. 5d). The grey clast-supported breccia is massive or thick-bedded, comprises angular grain-supported clasts with average size of 1–3 and at most ca. 10 cm within a shaly-sandy matrix. Clasts include mainly calcareous phyllites, some vein quartz and small micaschist pebbles. The thickness of the breccia is uncertain due to poor exposure but is estimated to reach at least 40 metres. The breccia represents a proximal alluvial facies and contrasts the conglomeratic facies exposed further to the east.
2. Red conglomerate lithofacies (Fig. 5c): The basal red lithostratigraphic unit comprises reddish hematite-rich

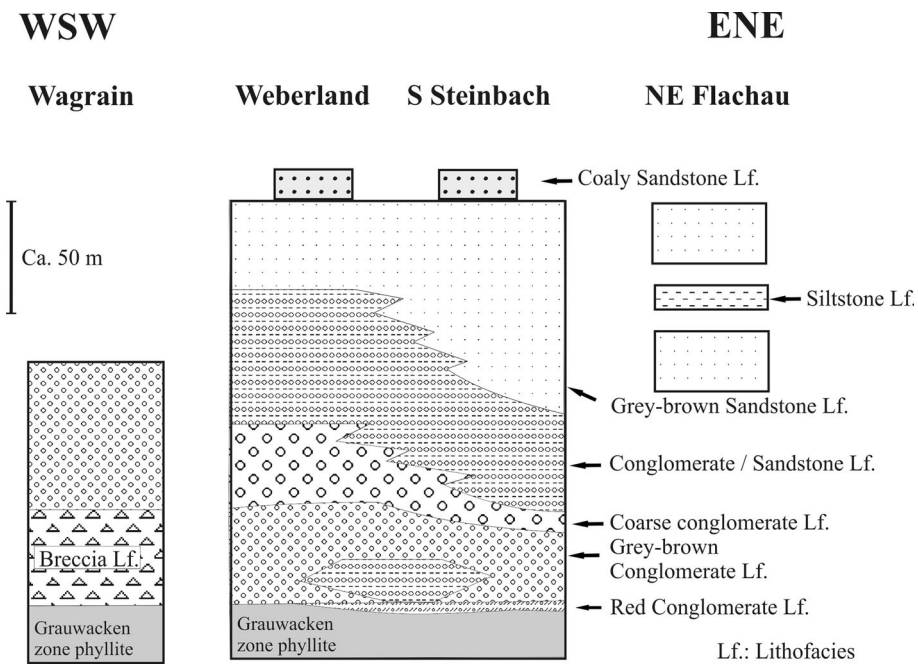

Fig. 6 Ca. ENE–WSW oriented lithofacies section of the Wagrain basin displaying vertical and lateral variations of lithofacies types. *Horizontal* and *vertical* proportions are not to scale

conglomerates and red mica-rich sandstones. The massive conglomerates comprise well-rounded reddish boulders and pebbles with a diameter reaching a maximum of ca. 30 cm. The clasts are coated by red hematite. The matrix comprises reddish sandstones and siltstones, which also occur as several centimetres thick lenses in the valley south of Steinbach (Fig. 3). These observations suggest a primary origin of the red conglomerate lithofacies. The red conglomerate lithofacies is ca. 3–8 metres thick and can be traced over approximately half the length of the basin (Fig. 3a). Hematite has been mined in the Steinbach area (Weber and Weiss 1983).

3. The overlying grey-brownish conglomerate lithofacies comprises a coarse-grained clast-supported conglomerate with variable clast sizes, ranging from a few centimetres to several decimetres (Fig. 5f). Clast size seems to increase upwards, and reaches a maximum of 50 cm in topmost layers, which form steep slopes. The clasts are well rounded or rounded according to the classification given in Füchtbauer (1988). The conglomerate is polymict and comprises mostly metamorphic basement rocks (see below). Locally, up to 30 cm thick mica-rich sandstone lenses are intercalated within conglomerate beds. The thickness of grey-brown conglomerates reaches ca. 80 m. Between Steinbach and Steinbachgraben, a ca. 20 m thick alternation of conglomerates and coarse-grained sandstones has been found between red and grey-brownish conglomerates. The individual beds are several centimetres to decimetres thick and also display some sedimentary structures including scour and fill structures (Fig. 5e).
4. Alternating conglomerate/sandstone lithofacies: Above the grey-brown conglomerates, an alternation of mica-rich well bedded sandstones and several metres thick conglomerates follow. Conglomerates comprise clasts with an average diameter of 1–4 cm, include only a few coarser clasts, and are dominated by vein quartz. The sandstones are mica-rich, relatively well sorted and show scour-and-fill structures. The thickness of this Conglomerate/sandstone unit reaches ca. 60 m and seemingly four cycles of sandstone/conglomerate alternations can be found.
5. Grey-brown sandstone lithofacies: Due to the disappearance of conglomerates, the alternating conglomerate/sandstone lithofacies grades into grey-brown pure mica-rich sandstones, which are well bedded. In the west, the whole sandstone succession is estimated to reach ca. 30 m in thickness, which increases towards the east.
6. Coaly sandstone lithofacies: Grey-brown sandstones grade into 6–8 m thick dark greyish to locally black, coaly sandstones, which are well exposed close to the middle station of the Wagrainer Höhe cable car. These sandstone beds are internally massive and ca. 10–60 cm thick.
7. Brownish siltstone lithofacies: Ca. eight metres thick siltstones were only found in one section in a gorge to the NE of Flachau, where these siltstones are intercalated within grey-brownish sandstones.

In summary, the overall distribution of clast/grain size shows that grain sizes decrease eastwards, and the only silt- and sandstones are found in the east. Furthermore, the

overall angularity of clasts decreases from west to east. Both types of observations indicate an overall eastward transport direction.

In several outcrops, a limited number of indicators for palaeo-transport directions have been found mainly in sandstone bodies (Fig. 3c). These are mainly oriented to the ESE respectively to WNW and S, showing a possible source in the WNW. This is in agreement with clast size and roundness, which show an eastward transport direction.

5 Provenance analysis of conglomerates

Conglomerates from several localities have been evaluated in respect to their clast composition (Table 1; Fig. 7). The composition varies from place to place. The breccia lithofacies mainly comprises calcareous phyllite and vein quartz, beside a low proportion of small micaschist and gneiss pebbles. Vein quartz, pegmatite gneiss and orthogneiss pebbles and boulders dominate the red conglomerate lithofacies.

The grey-brown conglomerate lithofacies is dominated by vein quartz, pegmatite and aplite gneiss and mica-poor, light-coloured orthogneiss and augengneiss. Among these, the orthogneiss and foliated pegmatite gneiss are particularly abundant components (Fig. 7). Quartzitic micaschist, greyish and light-coloured laminated/foliated mylonitic quartzites, garnet-rich paragneiss, and plagioclase amphibolite are other medium-grade metamorphic components. The orthogneiss clasts are similar to such exposed, e.g., in the Gneiss-Amphibolite Association of the Schladminger Tauern and Bösenstein massifs (Figs. 1, 2 for locations). Serpentinite (Fig. 6d), greenschist, black lydite, and dark phyllite pebble assemblages originate from low-grade metamorphic successions. Beside serpentinite, these clast assemblages are similar to those exposed in the nearby respectively underlying Grauwacken zone located to the north of the Wagrain basin. Serpentinite is common in the Hochgrößen unit, which is part of the Speik complex (Faryad et al. 2002). Subordinate clasts are red sandstone of the Werfen Formation type (Lower Triassic) and rare greyish dolomite from Middle to Upper Triassic formations of the Northern Calcareous Alps. The compositional maturity increases up-section indicated by increasing proportions of vein quartz and quartzitic schists (Fig. 7).

6 Sandstone petrography

Sandstone samples from various lithofacies types have been investigated. Sandstones from the basal red conglomerate lithofacies and of the overlying grey-brownish lithofacies show a number of significant differences. Sandstones of the red conglomerate lithofacies are mud-supported, comprise more than 80 percent matrix and include angular clasts in a reddish limonitic/hematitic matrix (Fig. 8a, b). Clasts comprise mono- and polycrystalline quartz, a few quartz grains with resorption similar to volcanic phenocrysts, abundant phyllitic clasts and subordinate white mica and very rare ghost crystals after biotite. The latter are entirely transformed crystals with no birefringence and include very fine-grained needles of Ti minerals indicating an originally biotite composition (Füchtbauer 1988; see also Rieser et al. 2005). Large K-feldspar crystals and microcrystalline volcanic matrix (Fig. 8b) occur occasionally. Isometric opaque minerals (likely magnetite) are other rare constituents. Feldspar, mostly K-feldspar, occurs only in a few grains. Quartz with resorption features, K-feldspar, ghost biotite grains and

Table 1 Composition of conglomerates from the Wagrain basin (values in percent)

	Basal Breccia	Red Conglomerate	Base coarse Conglomerate	High coarse Conglomerate	Conglomerate/sandstone
Intraformational sandstone	–	7	–	–	7
Quartz sandstone	8		–	–	–
Dolomite	–	2	–	4	–
Dark-grey phyllite	29	12	7	2	7
Bright calcareous phyllite	59	–	2	–	–
Dark quartzite	–	–	4	–	–
Vein quartz	4	20	26	36	38
Micaschist	–	20	13	12	3
Quartzitic schist	–	22	30	26	30
Orthogneiss	–	12	17	19	15
Pegmatite gneiss	–	5	1	1	–

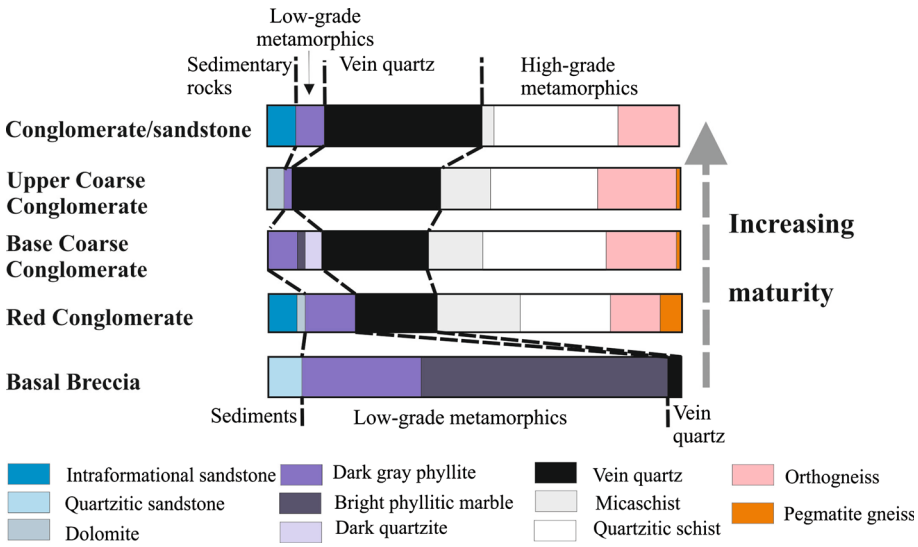

Fig. 7 Provenance analysis of conglomerates

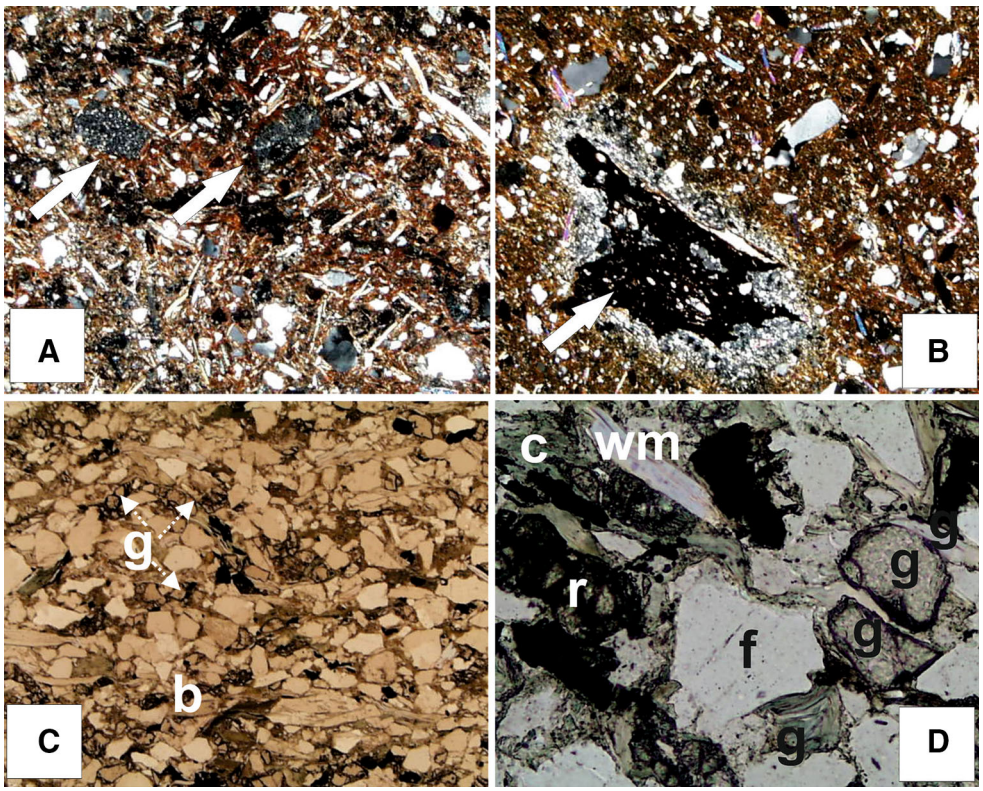

Fig. 8 Representative photomicrographs of sandstones from various formations within the Wagrain basin. **a**, **b** Samples from the basal *reddish* sandstones. *Arrows* in **a**, **b** indicate microcrystalline volcanic clasts. **c**, **d** *Grey-brownish* sandstone lithofacies rich in micas and translucent heavy minerals. *b* biotite, *c* chlorite, *g* garnet, *r* rutile, *wm* white mica

microcrystalline chards argue for a significant volcanic contribution of acidic composition in the red sandstones.

Representative samples of grey-brownish sandstones have been also evaluated according to the Dickinson-Gazzi method (Dickinson and Suczek 1979; Dickinson 1985). Ca. 400 points respectively 300 framework points of constituents (clasts larger than 0.063 mm) have been counted per sample. Results are shown in Table 2. The grey-brownish sandstones comprise subangular and rounded components, have a low proportion of shaley matrix (4.8–22.3 %) and are grain-supported. Clasts include mono-crystalline quartz, phyllitic metamorphic components, a high proportion of white mica reaching a maximum of ca. 32 percent among framework constituents, biotite (0.8–18.3 %), chlorite (0.8–6.5 %), a high proportion of translucent heavy minerals reaching in part 10 percent and more, and some opaque minerals. Translucent heavy minerals are dominated by garnet (80–90 % of all

Table 2 Composition of sandstones from the Wagrain basin

Sample	RS 12	RS 25	RS 26	RS 27	RS 28	RS 29	RS 30	RS 31	RS 32	RS 33	RS 34	RS 35
Q_m	31.7	38.0	23.8	46.5	49.5	29.8	22.8	51.4	46.3	44.5	41.0	20.3
Q_p	3.8	22.3	1.3	4.0	8.5	3.0	1.0	2	6.8	6.5	4.0	6.8
K	5.3	2.0	5.0	7.8	3.8	2	1.8	9.1	3.0	1.3	3.5	1.0
P	2.0	2.3	0.8	3.3	4.8	1.3	4	3.1	1.3	4.3	4.3	2.5
$lith_{sed}$	–	2.0	–	–	0.5	–	–	–	–	0.5	–	–
$lith_{meta}$	0.8	5.0	23.8	3.8	5	5.3	9	1.7	3.8	5.3	2.0	24.0
$lith_{volc}$	0.3	–	–	–	–	–	–	–	–	–	–	–
Mus	16	15.3	14.8	8.0	7.5	24	24.5	13.7	13.5	16.5	16.5	17.8
Bio	6.2	2.0	12.8	2.0	5.8	5.3	18.3	1.7	6.8	7.3	4.0	11.3
Chl	2.0	1.8	0.8	0.3	1.8	6.5	3.5	3.7	2	3.0	2.8	1.8
Opaque	2.2	0.8	0.8	–	–	1.0	1.3	0.6	0.8	–	2.3	0.5
HM_{transl}	5.2	4.0	0.5	17.0	3.3	1.8	2.3	2.9	8.3	9.0	10.5	0.5
Cb_m	–	–	–	–	–	–	–	–	–	–	–	–
Matrix	24.5	4.8	16.0	7.5	9.8	20.3	11.8	10.0	7.8	2.0	9.3	13.8

Sample no.	RS 36	RS 37	RS 38	RS 39	RS 40	RS 42	RS 43	RS 44	RS 45	RS 46	RS 59
Q_m	33.8	31	41.8	41	29.5	43.2	44.9	43.5	39.8	29.8	34.3
Q_p	5.8	1.8	7.0	3.5	0.8	3.7	9.1	2.3	3.0	3.8	5.3
K	1.5	0.8	2.8	3.3	0.8	4.67	2.6	4.3	1.0	2.8	2.3
P	2.8	1.3	7.3	4.3	1.8	2.6	1.1	2.5	2.0	2.5	2.0
$lith_{sed}$	–	–	–	–	–	–	–	–	–	–	–
$lith_{meta}$	16	2.8	5.3	3.3	3.8	5.7	6.0	3.0	3.4	0.8	10.3
$lith_{volc}$	–	–	–	–	–	–	1.4	–	–	–	0.3
Mus	15.3	32.3	14.5	20.5	24.5	18.3	15.1	14.8	9.8	27.3	17.5
Bio	5.8	6.8	3.3	4.8	1.5	2.9	0.9	4.3	0.8	8.5	1.3
Chl	2.8	2.3	4.0	1.3	1.5	2.6	4.9	3.5	7.8	3.0	1.3
Opaque	0.5	2.5	0.5	0.5	1.8	1.7	0.6	–	0.5	0.8	0.8
HM_{transl}	1.3	2.0	7.0	4.3	0.8	4.3	3.7	6.8	22.0	4.3	9.5
Cb_m	–	–	–	–	–	–	–	–	–	–	0.3
Matrix	14.8	16.8	6.8	13.5	22.3	10.6	9.7	15.3	10.3	16.8	15.3

Q_m monocrystalline quartz, *Q_p* polycrystalline quartz, *K* K-feldspar, *P* plagioclase, *$lith_{sed}$* lithic sedimentary, *$lith_{met}$* lithic metamorphic, *$lith_{volc}$* lithic volcanic, *Mus* white mica, *Bio* biotite, *Chl* chlorite, *HM_{transl}* translucent heavy minerals, *Cb_m* monocrystalline carbonate

translucent heavy minerals; Fig. 8c, d). Further translucent heavy mineral grains comprise clinozoisite, sphene, rutile and very rarely amphibole.

Consequently, differences between red and grey-brownish sandstone include: (1) roundness of clasts, where red sandstones contain angular clasts and subangular to round clasts are found in the grey-brownish sandstone; (2) the fabric with dominating mud-supported red sandstones and grain-supported grey-brownish sandstones, and (3) the preservation of high amounts of biotite as well as of garnet in grey-brownish sandstones.

The red sandstone is matrix-dominated and represents, therefore, a quartzwacke composition. The matrix of the grey-brownish sandstones is fine-grained clastic material (mainly siltstone) and the proportion is variable, classifying the samples as lithic/quartz arenite to lithic/quartz wackes according to the classification of Dott (1964).

Sandstone composition has also been evaluated by the Dickinson-Gazzi method. The proportion of white mica is extremely high, reaching values of ca. 30 percent among framework constituents. Monocrystalline and polycrystalline quartz grains dominate. The amount of lithic metamorphic clasts is high and feldspar is largely absent. These compositions classify these samples as cratonic interior and orogenic sources (only two discrimination diagrams are shown: Fig. 9a, b) according to diagrams proposed by Dickinson and Suczek (1979), Valloni and Zuffa (1984) and Dickinson (1985). Unusual is the high overall content of mica grains. We include white mica, biotite and chlorite in total mica contents. A variation

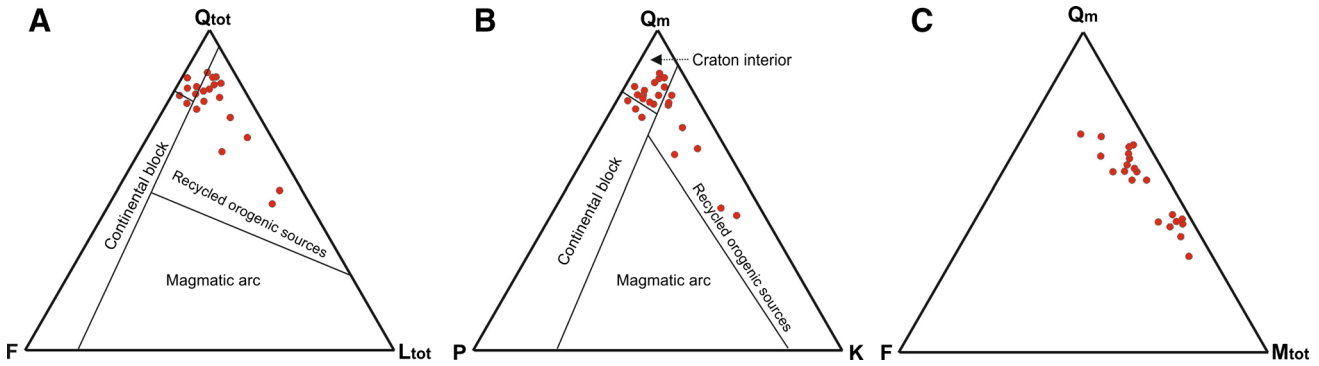

Fig. 9 **a**, **b** Sandstone discrimination diagrams proposed by Dickinson and Suzcek (1979). **a** Q_{tot}-F-L_{tot} diagram: Q_{tot} total quartz (monocrystalline and polycrystalline quartz), F feldspar, L_{tot} total lithics. **b** Q_m-P-K diagram: Q_m monocrystalline quartz, P plagioclase, K K-feldspar. **c** Variation of monocrystalline framework constituents: monocrystalline quartz (Q_m)—feldspar (F)—total mica (*Mtot* white mica + biotite + chlorite)

diagram of total mica, feldspar and monocrystalline quartz shows that mica comprises a high, but variable proportion of total white mica (Fig. 9c) compared to monocrystalline quartz. Mader and Neubauer (2004) attributed a molasse origin for sandstones with such high mica contents exceeding several percent among framework grains. Based on the relatively high monocrystalline quartz content, the classification to cratonic interior sources of ca. half of samples (Fig. 9b) is in part likely misleading because of the dilution of feldspar and lithic components by high mica and garnet contents, all indicating dominant medium-grade micaschist and subordinate gneissic sources. This gets obvious in diagram monocrystalline quartz vs. feldspar vs. mica (white mica, biotite, chlorite), which shows a wide range of monocrystalline quartz/mica ratios, in part with dominating white mica (Fig. 9c).

Variations between red and grey-brownish sandstones can be explained by a combination of tectonic, environmental and climatic factors. A difference arises in distinct weathering conditions in the source region because of nearly complete transformation of biotite into white mica. The variable roundness of e.g. monocrystalline quartz reflects varying duration and length of transport. This is in contrast to conglomerates, which are well rounded in both lithofacies types. Consequently, red sandstones were (more likely) deposited as mass flow within a wadi-type alluvial fan in contrast to fluvial-deltaic grey-brown sandstones. Finally, the high content of phyllitic clasts indicates a nearby source, e.g., within the underlying Grauwacken zone.

7 $^{40}Ar/^{39}Ar$ dating of detrital white mica

A mica-rich grey-brownish sandstone from a high lithostratigraphic level immediately beneath the coaly sandstones from a location (coordinates: N47°20′50″, E13°20′03″) at the artificial lake at the middle station of the Wagrain cable car has been chosen for single-grain $^{40}Ar/^{39}Ar$ analysis (sample RS-12). A grain size of 200–350 µm has been selected. The analytical technique is described in "Appendix 1" and follows that described in Rieser et al. (2006). A total of 24 single grains was measured. Analytical results of samples are reported in Table 3 and a summary of all single-grain ages is graphically displayed in Fig. 10 following the approach proposed by Sircombe (2004). Single-grain $^{40}Ar/^{39}Ar$ dating of detrital white mica yields an age peak between 85.9 ± 3.6 and 109.2 ± 4.9 with a majority around 100 Ma. One grain is younger (77.5 ± 3.3 Ma) and a few grains are slightly older (119.0 ± 5.9 Ma; 148.2 ± 11.1 Ma) and one grain is dated at 382.2 ± 7.5 Ma. The dominating Cretaceous-age population indicates a nearly exclusive origin of the dated detrital white mica from higher greenschist facies to medium-grade metamorphic rocks largely overprinted by eo-Alpine metamorphism. The recent experimental estimate of the Ar retention temperature is at 425 ± 25 °C for slow cooling rates (Harrison et al. 2009). Because of the grain size, pure phyllites with its typical grain size of white mica of ca. 100 µm can be excluded as a possible source.

8 Basin structure

The surface map data shows that the basin fill disconformably overlies the low-grade metamorphic rocks of the Grauwacken zone phyllites (Figs. 3a, 4). The structure of the basin is simple, and shows nearly uniform, gentle to intermediate ESE dip of the whole basin fill, which is cut, in the south, by the steeply N-dipping combined Mandling/Salzach-Enns faults. Internal faults are minor, and displacement is limited to offsets of several decimetres to metres. This fact is unexpected because the basin is

Table 3 $^{40}Ar/^{39}Ar$ analytical data of single-grain total fusion analysis

Grain no.	$^{36}Ar/^{39}Ar$ meas.	$\pm^{36}Ar/^{39}Ar$ 1-sigma abs.	$^{37}Ar/^{39}Ar$ irrad, corr.	$\pm^{37}Ar/^{39}Ar$ 1-sigma abs.	$^{40}Ar/^{39}Ar$ measured	$\pm^{40}Ar/^{39}Ar$ 1-sigma abs.	$\%^{40}Ar^*$	Age [Ma]	± [Ma]
Sample RS-12, detrital white mica grains, 200–350 µm, J value: 0.00585 ± 0.00003									
1	0.000024	0.003833	0.00011	0.13233	14.631	0.072	100.0	148.2	11.1
2	0.000011	0.001995	0.00033	0.08178	11.653	0.060	100.0	119.0	5.9
3	0.000004	0.000559	0.00024	0.03675	9.141	0.027	100.0	94.0	1.7
4	0.000003	0.000789	0.00032	0.04856	9.294	0.127	100.0	95.6	2.7
5	0.018053	0.002834	0.09978	0.14761	15.442	0.210	65.5	103.7	8.5
6	0.000005	0.000677	0.00027	0.03562	8.824	0.113	100.0	90.9	2.4
7	0.000010	0.001731	0.00053	0.05657	9.768	0.115	100.0	100.3	5.3
8	0.018532	0.002008	0.00000	0.00000	45.776	0.705	88.0	382.2	7.5
9	0.000001	0.001458	0.00054	0.07122	10.961	0.068	100.0	112.2	4.4
10	0.000009	0.001476	0.00048	0.06263	8.987	0.066	100.0	92.5	4.5
11	0.003553	0.001352	0.00139	0.18355	10.079	0.037	89.6	92.9	4.1
12	0.003912	0.001084	0.00112	0.14575	8.657	0.034	86.6	77.5	3.3
13	0.005172	0.001167	0.00082	0.15898	10.351	0.068	85.2	90.9	3.5
14	0.000034	0.001647	0.00140	0.28550	10.672	0.066	99.9	109.2	4.9
15	0.000008	0.001649	0.08454	0.24996	9.172	0.069	100.0	94.3	5.0
16	0.000006	0.001217	0.35622	0.15981	9.272	0.042	100.0	95.4	3.7
17	0.000013	0.002400	1.45512	0.30995	9.762	0.070	100.0	100.2	7.1
18	0.000972	0.001077	0.13623	0.21011	9.921	0.049	97.1	99.0	3.3
19	0.000831	0.002357	0.30725	0.43427	10.006	0.086	97.5	100.3	7.0
20	0.010429	0.004410	1.16234	0.79129	13.470	0.178	77.1	106.5	13.1
21	0.001593	0.001721	0.15565	0.23995	10.220	0.041	95.4	100.2	5.1
22	0.001837	0.001250	0.18512	0.23296	9.777	0.055	94.4	95.0	3.8
23	0.003214	0.001192	0.33767	0.23608	9.276	0.058	89.8	85.9	3.6
24	0.005600	0.001476	0.86929	0.33914	11.577	0.102	85.7	101.9	4.5

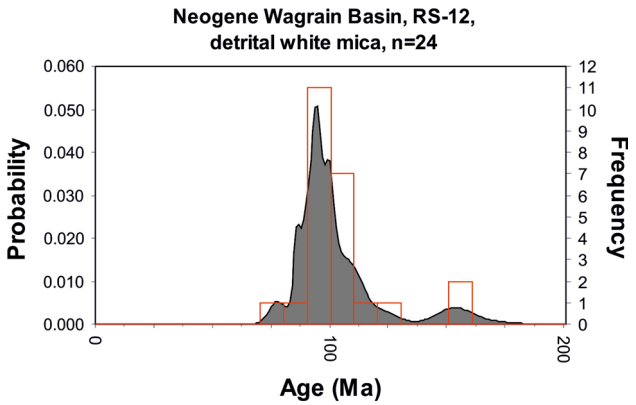

Fig. 10 Distribution of laser-probe single-grain $^{40}Ar/^{39}Ar$ ages of detrital white mica in a probability diagram after Sircombe (2004)

confined by the Mandling and Salzach-Enns faults, a major fault system with a displacement of 40 to a maximum of 60 km sinistral strike-slip offset, which has been estimated for the Salzach-Enns fault (Genser and Neubauer 1989; Ratschbacher et al. 1991; Frisch et al. 1998). In parts, the Salzach-Enns fault exposes several metres to ten metres thick black fault gouge (Heissel 1951; Mostler 1964; Exner 1996; Wang and Neubauer 1998).

To complete the study of Wang and Neubauer (1998), slickenside and striation data were collected at nine stations within the Wagrain basin fill between Wagrain and Altenmarkt (Fig. 11). Only a few faults per outcrop were found not allowing a systematic palaeostress evaluation, for which minimum four sets of faults are needed to deduce a palaeostress tensor. In two outcrops in metamorphic pre-Cenozoic basement rocks, superimposed sets of slickensides and striations indicate a polyphase reactivation of these faults (Wang and Neubauer 1998). Therefore, only representative examples are shown (Fig. 11).

1. Palaeostress tensor group A: The palaeostress tensor group A comprises E to ESE dipping normal faults, which in total yield WNW–ESE extension.

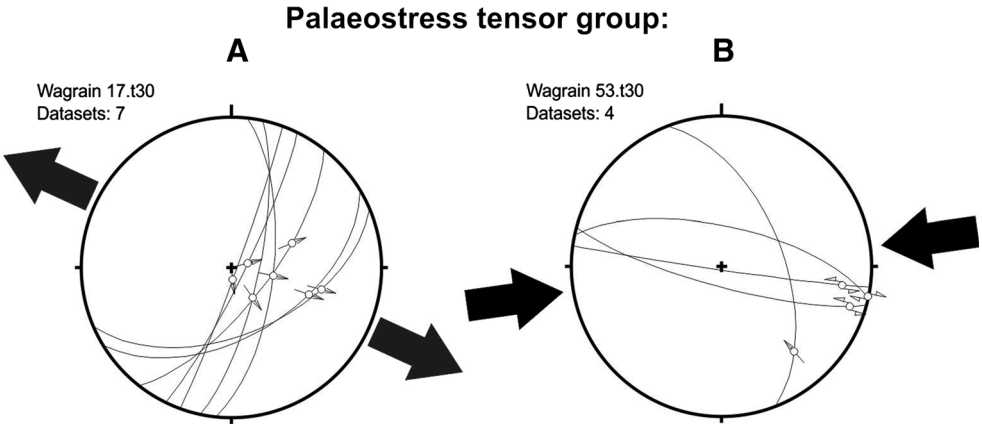

Fig. 11 Two examples of palaeostress patterns deduced from faults within the Wagrain basin

2. Palaeostress tensor group B comprises ca. E- to ESE-trending sinistral strike-slip faults. These can be explained by E–W compression.

Palaeostress tensor orientations deduced from faults within the surrounding metamorphic basement and within the Wagrain basin fill allow us to distinguish pre-basin and post-depositional palaeostress tensors (Wang and Neubauer 1998). This data is consistent with palaeostress development along the Tauern metamorphic core complex and shows an evolution from initial sinistral transpression over dextral transtension to post-depositional sinistral transpression and finally to dextral transpression.

9 Discussion

9.1 Formation mechanism of the Wagrain basin

The data presented above show that the Wagrain basin formed along the merging points of the two major regional, nearly orogen-parallel Salzach-Enns and Mandling faults. Together with the overall antiformal structure of the Grauwacken zone, this indicates that the Wagrain basin is now exposed in a halfgraben along the sinistral transtensional Salzach-Enns/Mandling fault system (Figs. 2, 3a). Several lines of evidence argue for this interpretation. In contrast to other regions, the underlying Grauwacken zone dips to the south and forms an overall antiform to the north of the Wagrain basin (Fig. 4, section A–A′). These relationships can be interpreted as a rollover structure due to N–S extension or transtension similar as proposed by Wang and Neubauer (1998) for the exhumation of Tauern metamorphic core complex. The overall sediment transport direction was axial along the basin towards the east, and N- and S-transport observed in outcrops could indicate a braided river system. This argues for a topographic gradient along the basin and the presence of a growing fault system, which is represented by the combined Salzach-Enns/Mandling fault system. Interestingly, the Wagrain basin represents the westernmost and structurally lowest elevation of scarcely preserved Miocene sedimentary units along the northern wall of the Mandling fault up to the Stoderzinken/Stoderalm area. The breccias, exposed in the west, are likely part of one or several mass flows from a local source (Grauwacken zone lithologies) exposed in the northwest.

9.2 Depositional age of the Wagrain basin

The exact age of the Wagrain basin fill is uncertain. The floral elements reported from the Wagrain basin do not really allow a clear biostratigraphic assignment of the basin fill (Steininger et al. 1988). Based on preserved flora, which originates from the coaly sandstone lithofacies, the uppermost preserved unit of the basin fill, Steininger et al. (1988) assumed a Karpatian age. The basin infill records a pronounced climate change from subtropical to a more humid temperate climate due to colour change from thin basal reddish, hematite-rich conglomerates to grey-brownish clastics. This change is used as a further argument for approximate dating as a similar, regional climate shift has been reported, e.g., from the Hieflau basin along the Salzach-Enns fault (Wagreich et al. 1997) and Styrian basin (see compilation of Ebner and Sachsenhofer 1995; Gross et al. 2007), and the age of the climatic shift is Ottnangian or pre-Ottnangian as Ottnangian coal bearing deposits are known in the Styrian basin (Gross et al. 2007). Similar reddish, but poorly dated deposits are also known from the area west of the Saualpe (Thiedig 1970; Kuhlemann et al. 2008), here also occurring at the base of the grey-brownish conglomerate or from the Tamsweg basin (Exner 1994; Zeilinger et al. 1999). Consequently, the colour transition could record the climate shift from a subtropical climate with terra rossa-type weathering to a more humid temperate climate, which predominated during

the Karpatian. A potentially Ottnangian-Karpatian age is, therefore, suggested for the red clastics of the Wagrain basin, in accordance with similar red soils in the Styrian, Hieflau and Tamsweg basins (Wagreich et al. 1997; Gross et al. 2007).

9.3 Source of the basin fill

The breccia at the western basin margin is derived from local sources and originates from the Grauwacken zone. The red sandstones reveal the influence of acidic volcanism. Such Early Miocene volcanism is widespread in the Pannonian and Transylvanian regions (e.g. Pécskay et al. 1995a, b) during Early and Middle Miocene (Karpatian to Badenian), and provides a further age constraint. Similar tuffaceous reddish clastic rocks are known in the Styrian basin, too (Gross et al. 2007).

Based on composition of grey-brownish conglomerates, sandstones and $^{40}Ar/^{39}Ar$ age distribution of white mica clasts, and the available detrital apatite fission track age of 50.0 ± 2.6 Ma (Dunkl et al. 2005) the peculiar composition allows deduce the provenance of the basin fill. The specific composition of clasts argues for the denudation of a medium-grade, gneissic terrain, although the clast composition represents the mature, transport-resistant components. The nearest medium-grade unit is the so-called Koppen Lamella exposed to the south of the Wagrain basin (Fig. 2; Exner 1991, 1996). We exclude the Koppen Lamella as a possible source for the following reasons: Its present exposure is very limited, too small in volume, and it comprises mainly amphibolite and ultramylonitic gneisses, which were not found in the Wagrain basin fill. Furthermore, it is simply not voluminous enough to explain the vast amount of material exposed in the Wagrain basin. Furthermore, Wagrain Phyllite from the footwall unit is missing, too. Such gneissic terrains, which are rich in pegmatite gneiss, can only be found in the Schladming and Bösenstein basement complexes, the Bösenstein complex is exposed ca. 40 respectively 80 km to the east of the present Wagrain basin (Figs. 2, 12). Furthermore, sandstones are extremely rich in garnet and coarse-grained white mica excluding phyllite as a source. The average $^{40}Ar/^{39}Ar$ age is ca. 100 Ma. This indicates an exclusive origin of dated detrital mica from rocks fully overprinted by eo-Alpine metamorphism. Such an overprint occurred in the Wölz Micaschist complex (Abart and Martinelli 1988; Schuster and Frank 1999; Schuster et al. 2001). Consequently, the Wölz Micaschist complex of Niedere Tauern (Fig. 2) is likely the main source, implying at least a ca. 40 km sinistral offset along the Salzach-Enns fault. We suppose, therefore, a provenance in the Bösenstein and eastern Wölz basement complexes, which would fit existing data, including: (1) The Bösenstein area exposes both deformed pegmatite gneisses in the Wölz Micaschist complex and various sorts of orthogneiss and augengneiss. (2) In contrast to the Schladming area with its apatite fission track ages of ca. 20–15 Ma (Frisch et al. 1998; Reinecker 2000), the Bösenstein area already cooled during the Eocene through ca. 100 °C-isotherm, as apatite fission track ages indicate (Hejl 1997, 1998). (3) The high white mica and garnet contents could have their origin in the spatially widespread Wölz Micaschist complex with its abundant garnet micaschists.

Furthermore, no typical rocks of the Lower Austroalpine nappe complex have been found, as e.g. greenish Alpine Verrucano-type quartz-phyllites and greenish quartzites of the Lantschfeld Formation. The lack of such clasts argues that this unit was not exposed at the surface during the time of Wagrain basin formation. This is in accordance with apatite fission track ages of ca. 20 Ma from the overlying Schladming unit (Hejl 1997, 1998; Reinecker, 2000), which indicates that Lower Austroalpine units must have been buried beneath the Schladming unit during the depositional time of the Wagrain basin.

The selected grain size for $^{40}Ar/^{39}Ar$ dating excludes phyllites of the Grauwacken zone as the main source for conglomerates and grey-brownish sandstones. Interestingly, there is only limited record of such sinistral strike-slip faults in the Wagrain basin.

A further remark is given to the composition of sandstones in general. The sandstones of the Wagrain basin are extremely mica-rich and belong to those with the highest proportions of mica within the framework constituents ever measured. Such mica-rich sandstones seem to be typical for late-stage orogenic, molasse-type sandstones as indicated by petrographic data from Variscan molasse (Mader and Neubauer 2004), and in rivers draining vast areas of plutonometamorphic basement, e.g. Amazonas in South America (Potter 1994). Mica-rich sands are often found in recent rivers in the axial, metamorphic zone of Alps (Garzanti et al. 2010). The same is true for high proportions of garnet, which is explained by exhumation of deeply subducted continental crust (Garzanti et al. 2010). In our case, the derivation is simply by denudation of a peculiar, widespread garnet-micaschist, which forms the main lithology within the Wölz Micaschist complex.

9.4 Structural evolution of the Wagrain basin

The data presented above suggests that the Wagrain basin formed along the merging points of two major regional, nearly orogen-parallel Salzach-Enns and Mandling faults. Together with the overall antiformal structure of the Grauwacken zone, this could indicate that the Wagrain basin formed in a halfgraben along the sinistral transtensional Salzach-Enns/Mandling fault system (Fig. 4).

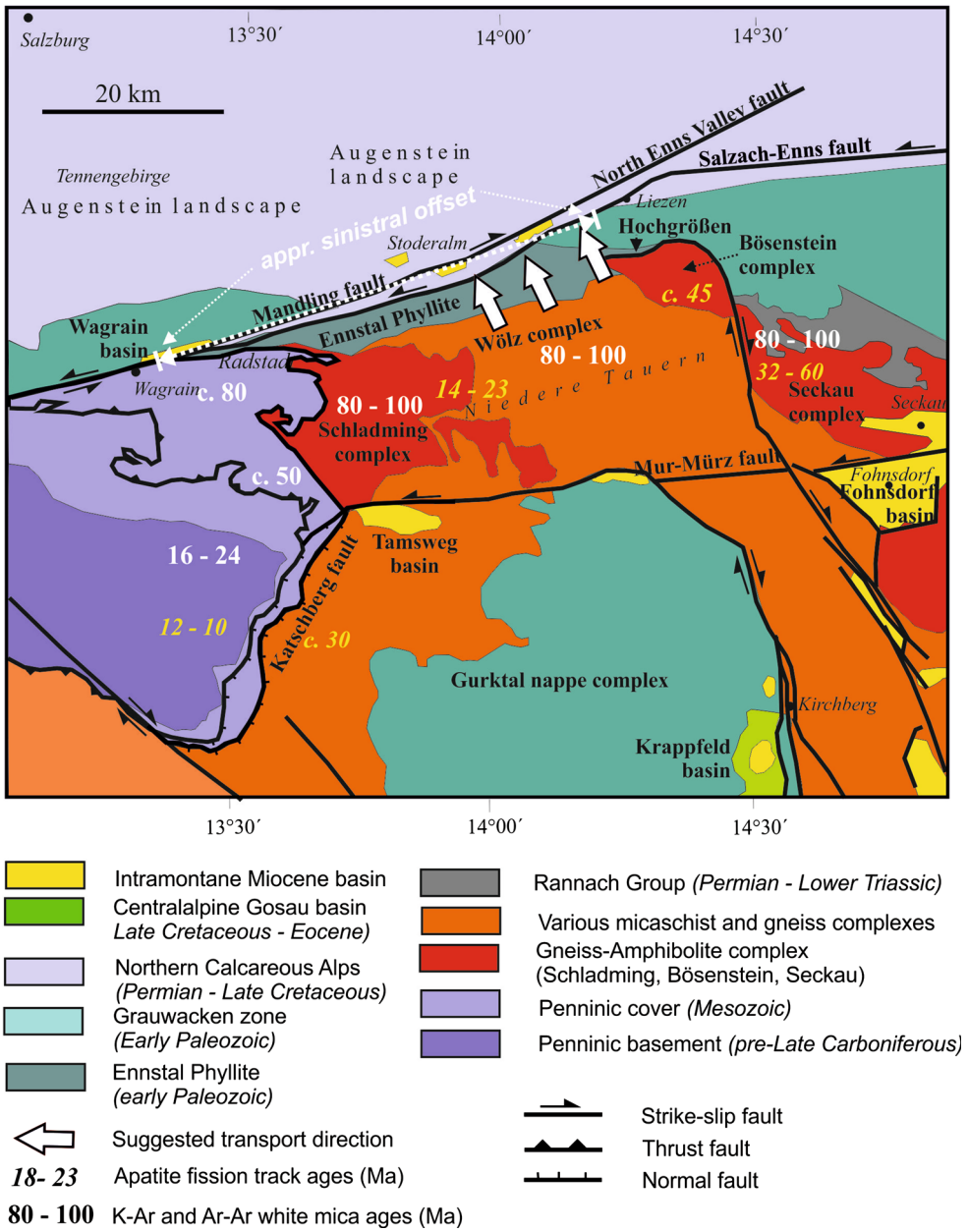

Fig. 12 Model of potential provenance in the eastern Niedere Tauern and Bösenstein areas for the Wagrain basin fill. Average K–Ar and Ar–Ar white mica ages are from Hejl (1984), Hejl et al. (1987), Abart and Martinelli (1988) and references in Pfingstl et al. (2015). Apatite fission track ages are compiled from Hejl (1997, 1998) and Reinecker (2000)

Several lines of evidence argue for this interpretation. In contrast to other regions, the underlying Grauwacken zone dips to the south and forms an overall antiform to the north of the Wagrain basin (Fig. 4, section A–A′). The remnant of the Wagrain basin fill is exposed at the southern termination of a rollover-type antiform. These structural relationships can be interpreted as a rollover structure due to approximately N–S extension or transtension. Other basins along the Salzach-Enns fault are transcurrent or pull-apart basins although structural details are not well known (Peresson and Decker 1997b; Wagreich et al. 1997; Keil and Neubauer 2011). A similar coeval Lower Miocene extensional or transtensional half-graben type basin is the Waldheimat basin further to the east (Neubauer and Unzog 2003).

In the Wagrain basin, the sediment transport direction is axial from the west respectively from the northwest, which argues for a topographic gradient and the presence of a growing fault system, which could be represented by the Salzach-Enns/Mandling fault system. Interestingly, the Wagrain basin represents the westernmost and structurally lowest elevation of scarcely preserved Lower Miocene sedimentary units along the northern wall of the Mandling fault. In combination with previous detailed results of palaeostress analysis along the Salzach-Enns fault of Wang and Neubauer (1998), the new results allow us to

distinguish pre-basin and post-depositional palaeostress tensors. This data is consistent with palaeostress development within and along the Tauern metamorphic core complex (Kurz et al. 1994; Wang and Neubauer 1998; Bertrand et al. 2015) and shows an evolution from initial sinistral transpression over dextral transtension to post-depositional sinistral transpression and finally to dextral transpression.

The transtensional nature of the Wagrain basin contrasts with some other intramontane basins of the Eastern Alps which are generally interpreted to represent pull-apart- and transcurrent basins along major strike-slip faults, e.g. the Mur-Mürz fault system (Nievoll 1985; Neubauer 1988; Ratschbacher et al. 1991; Zeilinger et al. 1999; Eder and Neubauer 2000). The Wagrain basin belongs to a group of basins, which formed along the northern margin (the northern margin is lateral) of the extrusional wedge (Wagreich et al. 1997). Not all of these basins are obviously controlled by strike-slip faults alone but normal faults play a major role, which indicate transtension nearly perpendicular to the motion direction of the extrusional wedge (Neubauer et al. 2000; Sachsenhofer et al. 2000; Strauss et al. 2001; Neubauer and Unzog 2003; Wagreich and Strauss 2005). In this sense, the Wagrain basin is thus an example of a transtensional basin related to the Mandling fault. Later on, the basin was inverted by E–W contraction.

Many further details of the overall Neogene relief development were demonstrated by Frisch et al. (1998) and Dunkl & Frisch (2002). In accordance with the interpretation given above, the Wagrain basin could be interpreted as part of the Dachstein peneplanation surface (Augenstein landscape) covering the whole eastern part of Northern Calcareous Alps and Central Alps (Frisch et al. 1998, 2001). However, the data show that there is no need for transport of clastic material across the Niedere Tauern area, and that the eastern Niedere Tauern block is one of the main sources of Lower Miocene basins and the data suggests that this area acted as a source. Furthermore, the distribution of Lower Miocene sedimentary rocks along the Mandling fault indicate that initial stages of orogen-parallel drainage may have already been established during the Early Miocene (Keil and Neubauer 2009), earlier as Frisch et al. (2000a, b) suggested.

Interestingly, only ESE–WNW extension and E–W compression has been found within the Wagrain basin, similar as already noted, based on only two exposures, by Wang and Neubauer (1998). The succession of these deformation events corresponds essentially to final deformation events found to the north within the Northern Calcareous Alps (Linzer et al. 1997; Peresson and Decker 1997a, b). Márton et al. (2000) found evidence for both major clockwise and anticlockwise rotations of Neogene basins in these sectors close to the northern margin of the extruding wedge, but significant counter-clockwise rotation of the Wagrain basin. These, in part structurally unresolved rotations might have been responsible for differences in detail in the structural evolution. However, the overall tectonic evolution seems to be similar all over the region.

9.5 Mandling wedge and other W-directed structures in Eastern Alps

The Mandling wedge exposed to the south of the Mandling fault can be explained as a dextral strike-slip duplex duplicating the Northern Calcareous Alps wedging into its Grauwacken zone basement (Figs. 2, 12). Using the offset of the base of Middle Triassic carbonates of the southern margin of the Northern Calcareous Alps in the northeast and western termination of carbonates of the Mandling wedge, the dextral offset along the Mandling fault is a minimum of 20 km. The age of dextral displacement along the present-day ENE-trending fault postdates the Wagrain basin fill.

Similar dextral E to ENE-trending faults have been found in other regions of the Eastern Alps. These include the ESE-trending Kaumberg fault separating the easternmost Northern Calcareous Alps from the Rhenodanubian flysch (Neubauer et al. 2006). Abundant hitherto unexplained sinistral N-trending strike-slip faults (e.g. in central sectors of the Eastern Alps; Neubauer 1988) along the central axis of the Eastern Alps predate ENE-trending sinistral extrusional related Neogene faults and can be explained with the same kinematic framework. These sinistral N–S trending faults are interpreted to represent the conjugate faults to the ENE-trending dextral faults constituting together conjugate Mohr shears ca. WSW-ENE strike-slip shortening, similar as proposed by outcrop-scale palaeostress analysis (Peresson and Decker 1997a, b).

Acknowledgments The author appreciates careful reviews by Bernd Lammerer and Michael Wagreich, which helped to clarify ideas and presentation. Fieldwork has been supported by a grant from the Austrian Science Fund FWF, project no. P9918-GEO as well as by the Austrian Geological Survey.

Appendix 1

$^{40}Ar/^{39}Ar$ analytical techniques largely follow descriptions given in Handler et al. (2004) with modifications used for single-grain dating in Rieser et al. (2006). Preparation of the samples before and after irradiation, $^{40}Ar/^{39}Ar$ analyses, and age calculations were carried out at the ARGONAUT Laboratory of the Institute for Geology and Palaeontology at the University Salzburg. Mineral concentrates are packed in aluminium-foil and placed in quartz vials. For calculation of the J-values, flux-monitors are placed between each 4–5

unknown samples, which yield a distance of ca. 5 mm between adjacent flux-monitors. The sealed quartz vials are irradiated in the MTA KFKI reactor (Debrecen, Hungary) for 16 h. Correction factors for interfering isotopes were calculated from 10 analyses of two Ca-glass samples and 22 analyses of two pure K-glass samples, and are: $^{36}Ar/^{37}Ar_{(Ca)} = 0.00026025$, $^{39}Ar/^{37}Ar_{(Ca)} = 0.00065014$, and $^{40}Ar/^{39}Ar_{(K)} = 0.015466$. Variation in the flux of neutrons was monitored with the DRA1 sanidine standard for which a $^{40}Ar/^{39}Ar$ plateau age of 25.03 ± 0.05 Ma has been reported (Wijbrans et al. 1995). After irradiation the minerals are taken from the quartz vials and the aluminium-foil packets, and handpicked into 1 mm diameter holes of the one-way Al-sample holders.

$^{40}Ar/^{39}Ar$ analyses are carried out using a UHV Ar-extraction line equipped with a combined MERCHANTEK™ UV/IR laser system, and a VG-ISOTECH™ NG3600 mass spectrometer.

Heating analyses, until fusion of single white mica grains are performed using a defocused (~1.5 mm diameter) 25 W CO_2-IR laser operating in Tem_{00} mode at wavelengths between 10.57 and 10.63 μm. The laser is controlled from a PC, and the position of the laser on the sample is monitored on the computer screen via a video camera in the optical axis of the laser beam through a double-vacuum window on the sample chamber. Gas clean-up is performed using one hot and one cold Zr-Al SAES getter. Gas admittance and pumping of the mass spectrometer and the Ar-extraction line are computer controlled using pneumatic valves. The NG3600 is an 18 cm radius 60° extended geometry instrument, equipped with a bright Nier-type source operated at 4.5 kV. Measurements are performed on an axial electron multiplier in static mode, peak-jumping and stability of the magnet is controlled by a Hall-probe. For each increment the intensities of ^{36}Ar, ^{37}Ar, ^{38}Ar, ^{39}Ar, and ^{40}Ar are measured, the baseline readings on mass 35.5 are automatically subtracted. Intensities of the peaks are back-extrapolated over 16 measured intensities to the time of gas admittance either by a straight line or a curved fit, depending on intensity and type of pattern of the evolving gas. Intensities are corrected for system blanks, background, post-irradiation decay of ^{37}Ar, and interfering isotopes. Isotopic ratios, ages and errors for individual measurements are calculated following suggestions by McDougall and Harrison (1999) using decay factors reported by Steiger and Jäger (1977).

References

Abart, R., & Martinelli, W. (1988). Variszische und alpidische Entwicklungsgeschichte des Wölzer Kristallins. *Mitteilungen der Geologie- und Bergbaustudenten Österreichs, 37*, 1–14.

Allen, P. A., & Allen, J. R. (1990). *Basin analysis*. Oxford: Blackwell Scientific Publishing.

Bergerat, F. (1989). From pull-apart to the rifting process: The formation of the Pannonian basin. *Tectonophysics, 157*, 271–280.

Bertrand, A., Rosenberg, C., & Garcia, S. (2015). Fault slip analysis and late exhumation of the Tauern Window, Eastern Alps. *Tectonophysics, 649*, 1–17.

Buchroithner, M.F. (1984). *Karte der Landsat-Bildlineamente von Österreich 1: 500.000, samt Erläuterungen*. 16 p., 1 map, Geologische Bundesanstalt, Vienna.

Cunningham, W. D., & Mann, P. (2007). Tectonics of strike-slip restraining and releasing bends. In W. D. Cunningham & P. Mann (Eds.), *Tectonics of Strike-slip Restraining and Releasing Bends*. Geological Society Special Publication (vol. 290, pp. 1–12). London: Geological Society of London.

Dickinson, W. R. (1985). Interpreting provenance relations from detrital modes of sandstones. In G. G. Zuffa (Ed.), *Provenance of Arenites* (pp. 333–362). Dordrecht: Reidel Publishing Co.

Dickinson, W. R., & Suczek, C. A. (1979). Plate tectonics and sandstone compositions. *American Association of Petroleum Geologists Bulletin, 63*, 2164–2182.

Dott, R. H. (1964). Wacke, graywacke and matrix—what approach to immature sandstone classification? *Journal of Sedimentary Petrology, 34*, 625–632.

Dunkl, I., & Frisch, W. (2002). Thermochronologic constraints on the Late Cenozoic exhumation along the Alpine and West Carpathian margins of the Pannonian basin. *EGU Stephan Mueller Special Publication Series, 3*, 135–147.

Dunkl, I., Kuhlemann, J., Reinecker, J., & Frisch, W. (2005). Cenozoic relief evolution of the Eastern Alps—constraints from apatite fission track age-provenance of Neogene intramontane sediments. *Austrian Journal of Earth Sciences, 98*, 92–105.

Ebner, F., & Sachsenhofer, R. E. (1995). Paleogeography, subsidence and thermal history of the Neogene Styrian Basin (Pannonian basin system, Austria). *Tectonophysics, 242*, 133–150.

Eder, N., & Neubauer, F. (2000). On the edge of the extruding wedge: Neogene kinematics and geomorphology along the southern Niedere Tauern, Eastern Alps. *Eclogae Geologicae Helvetiae, 93*, 81–92.

Einsele, G. (1992). *Sedimentary Basins* (p. 628). Berlin: Evolution, Facies and Sediment Budget, Springer-Verlag.

Exner, C. (1991). Lamellen von Gneis und Metabasit im Quarzphyllit der Nördlichen Radstädter Tauern (Salzburg). *Anzeiger der Österreichische Akademie der Wissenschaften mathematisch-naturwissenschaftliche Klasse, 1991*, 109–112.

Exner, C. (1994). Geologie des Schwarzenberges bei Tamsweg (Lungau, Salzburg). *Jahrbuch der Geologischen Bundesanstalt, 137*, 227–243.

Exner, C. (1996). Leitgesteine und Tektonik in Phylliten bei Wagrain und Radstadt (Land Salzburg). *Jahrbuch der Geologischen Bundesanstalt, 139*, 155–190.

Faryad, S. W., Melcher, F., Hoinkes, G., Puhl, J., Meisel, T., & Frank, W. (2002). Relics of eclogite facies metamorphism in the Austroalpine basement, Hochgrössen (Speik complex), Austria. *Mineralogy and Petrology, 74*, 49–73.

Fodor, L. (1995). From transpression to transtension: Oligocene-Miocene tectonic evolution of the Vienna basin and the East Alpine-Western Carpathian junction. *Tectonophysics, 242*, 151–182.

Fodor, L., Csontos, L., Bada, G., Györfi, I., & Benkovics L. (1999). Tertiary tectonic evolution of the Pannonian Basin system and neighbouring orogens: a new synthesis of palaeostress data. In: B. Durand, L. Jolivet, F. Horváth & M. Seranne (Eds.) *The Mediterranean Basins: Tertiary Extension within the Alpine*

Orogen. Geological Society Special Publication (vol. 156, pp. 295–334). London: Geological Society of London.

Frank, W., & Schlager, W. (2006). Jurassic strike-slip versus subduction in the Eastern Alps. *International Journal of Earth Sciences, 95*, 431–450.

Friebe, J. (1991). Neotektonik an der Mittelsteirischen Schwelle (Österreich): Die "Steirische" Phase. *Zentralblatt für Geologie und Paläontologie Teil I, 1991*, 41–54.

Frisch, W., Kuhlemann, J., Dunkl, I., & Brügel, A. (1998). Palinspastic reconstruction and topographic evolution of the Eastern Alps during late Tertiary tectonic extrusion. *Tectonophysics, 297*, 1–15.

Frisch, W., Dunkl, I., & Kuhlemann, J. (2000a). Post-collisional orogen-parallel large-scale extension in the Eastern Alps. *Tectonophysics, 327*, 239–265.

Frisch, W., Székely, B., & Kuhlmann, J. (2000b). Geomorphological evolution of the Eastern Alps in response to Miocene tectonics. *Geomorphologie, 44*(1), 103–138.

Frisch, W., Kuhlemann, J., Dunkl, I., & Székely, B. (2001). The Dachstein paleosurface and the Augenstein Formation in the Northern Calcareous Alps—a mosaic stone in the geomorphological evolution of the Eastern Alps. *Internal Journal of Earth Sciences, 90*, 500–518.

Frost, E., Dolan, J., Ratschbacher, L., Hacker, B., & Seward, G. (2011). Direct observation of fault zone structure at the brittle-ductile transition along the Salzach–Ennstal–Mariazell–Puchberg fault system, Austrian Alps. *Journal of Geophysical Research, 116*, B02411. doi:10.1029/2010JB007719.

Füchtbauer, H. (1988). *Sedimente und Sedimentgesteine*. vol. 2. 4th edn, Stuttgart: Schweizerbart, XVI + p. 1141.

Garzanti, E., Resentini, A., Vezzoli, G., Andò, S., Malusà, M. G., Padoan, M., & Paparella, P. (2010). Detrital fingerprints of fossil continental-subduction zones (Axial Belt Provenance, European Alps). *Journal of Geology, 118*, 341–362.

Genser, H., & Neubauer, F. (1989). Low angle normal faults at the eastern margin of the Tauern window (Eastern Alps). *Mitteilungen der Österreichischen Geologischen Gesellschaft, 81*(1988), 233–243.

Gross, M., Fritz, I., Piller, W. E., Soliman, A., Harzhauser, M., Hubmann, B., et al. (2007). The Neogene of the Styrian basin—guide to excursions. *Joannea Geologie und Paläontologie, 9*, 117–193.

Handler, R., Neubauer, F., Velichkova, S. H., & Ivanov, Z. (2004). $^{40}Ar/^{39}Ar$ age constraints on the timing of magmatism and post-magmatic cooling in the Panagyurishte region, Bulgaria. *Schweizerische Mineralogische und Petrographische Mitteilungen, 84*, 119–132.

Harrison, T. M., Célérier, J., Aikman, A. B., Hermann, J., & Heizler, M. T. (2009). Diffusion of ^{40}Ar in muscovite. *Geochimica et Cosmochimica Acta, 73*, 1039–1051.

Heissel, W. (1951). Grauwackenzone der Salzburger Alpen. *Verhandlungen der Geologischen Bundesanstalt (Wien) Sonderheft A* (1950/51), 71–76.

Hejl, E. (1984). Geochronologische und petrologische Beiträge zur Gesteinsmetamorphose der Schladminger Tauern. *Mitteilungen der Geologie- und Bergbaustudenten Österreichs, 30*(31), 289–318.

Hejl, E. (1997). 'Cold spots' during the Cenozoic evolution of the Eastern Alps: Thermochronological interpretation of apatite fission-track data. *Tectonophysics, 272*, 159–172.

Hejl, E. (1998). Über die känozoische Abkühlung und Denudation der Zentralapen östlich der Hohen Tauern—eine Apatit-Spaltspuranalyse. *Mitteilungen der Österreichischen Geologischen Gesellschaft, 89*(1996), 179–199.

Hejl, E., Rockenschaub, M., & Slapansky, P. (1987). Geochronologische Daten aus den Schladminger Tauern und ihre geologische Interpretation. *Arbeitstagung der Geologischen Bundesanstalt 1987 Blatt 127 Schladming* (pp. 94–102), Wien: Geologische Bundesanstalt.

Hirschberg, K.J. (1965). *Die Geologie des Mandlingzuges (Oberes Ennstal, Österreich)*. Doktoral Thesis University of Marburg/Lahn, p. 110.

Keil, M., & Neubauer, F. (2009). Initiation and development of a fault-controlled, orogen-parallel overdeepened valley). The Upper Enns Valley, Austria. *Austrian Journal of Earth Sciences, 102*, 80–90.

Keil, M., & Neubauer, F. (2011). The Miocene Enns Valley basin (Austria) and the North Enns Valley fault. *Austrian Journal of Earth Sciences, 104*, 49–65.

Kuhlemann, J., Frisch, W., Dunkl, I., & Székely, B. (2001a). Quantifying tectonic versus erosive denudation by the sediment budget: Miocene core complexes of the Alps. *Tectonophysics, 330*, 1–23.

Kuhlemann, J., Frisch, W., Dunkl, I., Székely, B., & Spiegel, C. (2001b). Miocene shifts of the drainage divide in the Alps and their foreland basin. *Geomorphologie, 45*(2), 239–265.

Kuhlemann, J., Taubold, H., Vennemann, T., Dunkl, I., & Frisch, W. (2008). Clay mineral and geochemical composition of Cenozoic paleosol in the Eastern Alps (Austria). *Austrian Journal of Earth Sciences, 101*, 60–69.

Kurz, W., Neubauer, F., Genser, J., & Horner, H. (1994). Sequence of Tertiary brittle deformations in the eastern Tauern Window, Eastern Alps. *Mitteilungen der Österreichischen Geologischen Gesellschaft, 86*, 153–164.

Leeder, M. (1999). *Sedimentology and Sedimentary Basins. From Turbulence to Tectonics* (p. 592). Oxford: Blackwell Science.

Linzer, H. G., Moser, F., Nemes, F., Ratschbacher, L., & Sperner, B. (1997). Build-up and dismembering of the eastern Northern Calcareous Alps. *Tectonophysics, 272*, 97–124.

Liu, Y., Genser, J., Handler, R., Friedl, G., & Neubauer, F. (2001). $^{40}Ar/^{39}Ar$ muscovite ages from the Penninic/Austroalpine plate boundary, Eastern Alps. *Tectonics, 20*, 528–547.

Mader, D., & Neubauer, F. (2004). Provenance of Palaeozoic sandstones from the Carnic Alps (Austria): Petrographic and geochemical indicators. *International Journal of Earth Sciences, 93*, 262–281.

Mandl, G. W., Hejl, Ewald, Van Husen, D., Ahl, A., Draxler, I., Heinrich, M., et al. (2014). *Erläuterungen zu Blatt 127 Schladming* (p. 87). Wien: Geologische Bundesanstalt.

Márton, E., Kuhlemann, J., Frisch, W., & Dunkl, I. (2000). Miocene rotations in the Eastern Alps—palaeomagnetic results from intramontane basin sediments. *Tectonophysics, 323*, 163–182.

McDougall, I., & Harrison, M.T. (1999). *Geochronology and Thermochronology by the $^{40}Ar/^{39}Ar$ Method*, 2nd edn. Oxford: Oxford University Press.

Mostler, H. (1964). Einige Bemerkungen zur Salzach-Längstalstörung und der sie begleitenden Gesteine (im Bereich Wagrain bis Lend, Salzburg). *Mitteilungen der Geologie- und Bergbaustudenten in Wien, 14/15*, 185–196.

Neubauer, F. (1988). Bau und Entwicklungsgeschichte des Rennfeld-Mugel- und des Gleinalmkristallins (Ostalpen). *Abhandlungen der Geologischen Bundesanstalt, 42*, 1–137.

Neubauer, F., & Genser, J. (1990). Architektur und Kinematik der östlichen Zentralalpen—eine Übersicht. *Mitteilungen des Naturwissenschaftlichen Vereins für Steiermark, 120*, 203–219.

Neubauer, F., Genser, J., & Handler, R. (2000). The Eastern Alps: Result of a two-stage collision process. *Mitteilungen der Österreichischen Geologischen Gesellschaft, 92*, 117–134.

Neubauer, F., Genser, J., Kurz, W., & Wang, X. (1999). Exhumation of the Tauern window, Eastern Alps. *Physics and Chemistry of Earth Part A: Solid Earth and Geodesy, 24*, 675–680.

Neubauer, F., Genser, J., & Pointner, P. (2006). Palaeogene–Early Miocene collisional structures of Eastern Alps and motion of Adria. *Geophysical Research Abstracts*, 8, EGU06-A-06682.

Neubauer, F., & Unzog, W. (2003). Halfgraben formation within an extruding wedge: the Neogene Waldheimat basin in the Eastern Alps. *Neues Jahrbuch für Geologie und Paläontologie Abhandlungen, 230*, 133–154.

Nievoll, J. (1985). Die bruchhafte Tektonik entlang der Trofaiachlinie (Östliche Zentralalpen, Österreich). *Jahrbuch der Geologischen Bundesanstalt, 127*, 643–671.

Ortner, H. & Stingl, V. (2001). Facies and Basin Development of the Oligocene in the Lower Inn Valley, Tyrol/Bavaria. In: Piller, W. & Rasser, M. (Eds.), *Paleogene in Austria. Schriftenreihe der Erdwissenschaftlichen Kommission* (vol. 14, pp. 153–196). Wien: Österreichische Akademie der Wissenschaften.

Pécskay, Z., Edelstein, O., Seghedi, I., Szakács, A., Lexa, J., Kováčs, M., et al. (1995a). K-Ar datings of Neogene-Quaternary calc-alkaline volcanic rocks in Romanian. *Acta Vulcanologica, 7*, 53–61.

Pécskay, Z., Lexa, J., Szkács, A., Balogh, K., Seghedi, I., Konecny, V., et al. (1995b). Space and time distribution of Neogene-Quaternary volcanism in the Carpatho-Pannonian Region. *Acta Vulcanologica, 7*, 15–28.

Peresson, H., & Decker, K. (1997a). Far-field effects of Late Miocene subduction in the Eastern Carpathians: E-W compression and inversion of structures in the Alpine–Carpathian–Pannonian region. *Tectonics, 16*, 38–56.

Peresson, H., & Decker, K. (1997b). The Tertiary dynamics of the northern Eastern Alps (Austria): changing palaeostress in a collisional plate boundary. *Tectonophysics, 272*, 125–157.

Petrascheck, W. (1924). Braunkohlenlager der österreichischen Alpen. *Berg- und hüttenmännisches Jahrbuch, 72*, 5–48.

Petrascheck, W. (1937). Die Kohlenlager Österreichs. *Zeitschrift für Berg-, Hütten- und Salinenwesen, 85*, 179–186.

Pfingstl, S., Kurz, W., Schuster, R., & Hauzenberger, C. (2015). Geochronological constraints on the exhumation of the Austroalpine Seckau Nappe (Eastern Alps). *Austrian Journal of Earth Sciences, 108*, 174–187.

Piller, W. E., Harzhauser, M., & Mandic, O. (2007). Miocene Central Paratethys stratigraphy—current status and future directions. *Stratigraphy, 4*, 151–168.

Potter, P. E. (1994). Modern sands of South America: Composition, provenance and global significance. *Geologische Rundschau, 83*, 212–232.

Ratschbacher, L., Frisch, W., Linzer, G., & Merle, O. (1991). Lateral extrusion in the Eastern Alps, part 2: Structural analysis. *Tectonics, 10*, 257–271.

Ratschbacher, L., Frisch, W., Neubauer, F., Schmid, S. M., & Neugebauer, J. (1989). Extension in compressional orogenic belts: The Eastern Alps. *Geology, 17*, 404–407.

Reinecker, J. (2000). Stress and deformation: Miocene to present-day tectonics in the Eastern Alps. Tübinger Geowissenschaftliche Arbeiten (TGA) Reihe A: Geologie, Paläontologie, Stratigraphie (p. 124). Tübingen: Eberhard Karls-Universität Tübingen.

Rieser, A. B., Liu, Y., Genser, J., Neubauer, F., Handler, R., Friedl, G., & Ge, X. H. (2006). $^{40}Ar/^{39}Ar$ ages of detrital white mica constrain the Cenozoic development of the intracontinental Qaidam Basin, China. *Geological Society of America Bulletin, 118*, 1522–1534.

Rieser, A., Neubauer, F., Liu, Y., & Ge, X. (2005). Sandstone provenance of north-western sectors of the intracontinental Cenozoic Qaidam basin, western China: Tectonic vs. climatic control. *Sedimentary Geology, 177*, 1–18.

Robl, J., Hergarten, S., & Stüwe, K. (2008a). Morphological analysis of the drainage system in the Eastern Alps. *Tectonophysics, 460*, 263–277.

Robl, J., Stüwe, K., Hergarten, S., & Evans, L. (2008b). Extension during continental convergence in the Eastern Alps: The influence of orogen-scale strike-slip faults. *Geology, 36*, 963–966.

Royden, L. H. (1985). The Vienna Basin: A thin-skinned pull-apart basin. *Special Publication Society of Economic Paleontologists and Mineralogists, 37*, 319–338.

Royden, L. (1988). Late Cenozoic tectonics of the Pannonian basin system. *American Association of Petroleum Geologists Memoir, 45*, 1–25.

Sachsenhofer, R. F. (1988). Zur Inkohlung des Ennstaltertiärs. *Sitzungsberichte Österreichische Akademie der Wissenschaften mathematisch-naturwissenschaftliche Klasse Abt. I, 197*, 333–342.

Sachsenhofer, R., Kogler, A., Polesny, H., Strauss, P., & Wagreich, M. (2000). The Neogene Fohnsdorf Basin: Basin formation and basin inversion during lateral extrusion in the Eastern Alps (Austria). *Internal Journal of Earth Sciences, 89*, 415–430.

Sachsenhofer, R. F., Lankreijer, A., Cloetingh, S., & Ebner, F. (1997). Subsidence analysis and quantitative basin modelling in the Styrian Basin (Pannonian Basin System, Austria). *Tectonophysics, 272*, 175–196.

Scharf, A., Handy, M. R., Favaro, S., Schmid, S. M., & Bertrand, A. (2013). Modes of orogen-parallel stretching and extensional exhumation in response to microplate indentation and roll-back subduction (Tauern Window, Eastern Alps). *International Journal of Earth Sciences, 102*, 1627–1654.

Schmidlechner, M., Neubauer, F., & Handler, R. (2006). Extent and age of metamorphism of the central Grauwacken Zone, Eastern Alps: A $^{40}Ar/^{39}Ar$ study. Pangeo Austria 2006. Conference Series (pp. 314–315). Innsbruck: Innsbruck University Press.

Schönlaub, H. P. (1975). Zum Alter der Radstädter Quarzphyllite (Unterostalpin, Salzburg). *Annalen des Naturhistorischen Museums Wien, 79*, 47–55.

Schönlaub, H. P. (1979). Das Paläozoikum in Österreich. Verbreitung, Stratigraphie, Korrelation, Entwicklung und Paläogeographie nichtmetamorpher und metamorpher Abfolgen. *Abhandlungen der Geologischen Bundesanstalt, 29*, 1–124.

Schuster, R., & Frank, W. (1999). Metamorphic evolution of the Austroalpine units east of the Tauern Window: indications for Jurassic strike slip tectonics. *Mitteilungen der Geologie- und Bergbaustudenten Österreichs, 42*, 37–58.

Schuster, R., Scharbert, S., Abart, R., & Frank, W. (2001). Permo-Triassic extension and related HAT/LP metamorphism in the Austroalpine—Southalpine realm. *Mitteilungen der Geologie- und Bergbaustudenten Österreichs, 45*, 111–141.

Seguret, M., Seranne, M., Chauvet, A. B. M., & Brunel, A. (1989). Collapse basin: a new type of extensional sedimentary basin from the Devonian of Norway. *Geology, 17*, 127–130.

Sircombe, K. N. (2004). AgeDisplay: An EXCEL workbook to evaluate and display univariate geochronological data using binned frequency histograms and probability density distributions. *Computer & Geosciences, 30*, 21–31.

Steiger, R. H., & Jäger, E. (1977). Subcommission on geochronology: Convention on the use of decay constants in geo- and cosmochronology. *Earth and Planetary Science Letters, 36*, 359–362.

Steininger, F. F., Rögl, F., Hochuli, P., & Müller, C. (1988). Lignite deposition and marine cycles. The Austrian Tertiary lignite deposits. A case history. *Österreichische Akademie der Wissenschaften Sitzungsberichte mathematisch-naturwissenschaftliche Klasse Abt. 1, 197*, 309–332.

Strauss, P., Wagreich, M., Decker, K., & Sachsenhofer, R. F. (2001). Tectonics and sedimentation in the Fohnsdorf-Seckau Basin (Miocene, Austria): from a pull-apart basin to a half-graben. *International Journal of Earth Sciences, 90*, 549–559.

Sylvester, A. G. (1988). Strike-slip faults. *Geological Society of America Bulletin, 100*, 1666–1703.

Thiedig, F. (1970). Verbreitung. Ausbildung und stratigraphische Einstufung neogener Rotlehme und Grobschotter in Ostkärnten (Osterreich). *Mitteilungen des Geologisch-Paläontäontologischen Instituts der Universität Hamburg*, 38, 97–116.

Tollmann, A. (1985). *Geologie von Österreich, Band II. Außerzentralalpiner Anteil* (p. 710). Wien: Deuticke.

Trauth, F. (1918). Das Eozänvorkommen bei Radstadt im Pongau. *Österreichische Akademie der Wissenschaften mathematisch-naturwissenschaftlichen Klasse Denkschriften,* 95, 171–278.

Trauth, F. (1925). Geologie der Nördlichen Radstädter Tauern und ihres Vorlandes 1. Teil. *Österreichische Akademie der Wissenschaften mathematisch-naturwissenschaftlichen Klasse Denkschriften*, 100, 101–212.

Trauth, F. (1927). Geologie der Nördlichen Radstädter Tauern und ihres Vorlandes. 2. Teil. *Österreichische Akademie der Wissenschaften mathematisch-naturwissenschaftlichen Klasse Denkschriften*, 101, 29–65.

Valloni, R., & Zuffa, G. G. (1984). Provenance changes for arenaceous formations of the northern Apennines, Italy. *Geological Society of America Bulletin, 95*, 1035–1039.

Wagreich, M. & Strauss, P.E. (2005). Source area and tectonic control on alluvial fan development in the Miocene Fohnsdorf intramontane basin, Austria. In: A.M. Harvey, A. E. Mather. & M. Stokes (Eds.), *Alluvial Fans: Geomorphology, Sedimentology, Dynamic*s (vol. 251, pp. 207–216). London: Geological Society [London] Special Publication.

Wagreich, M., Zetter, R., Bryda, G., & Peresson, H. (1997). Das Tertiär von Hieflau (Steiermark): Untermiozäne Sedimentation in den östlichen Kalkalpen. *Zentralblatt für Geologie- und Paläontologie Teil I, 1996*, 633–645.

Wang, X., & Neubauer, F. (1998). Orogen-parallel strike-slip faults bordering metamorphic core complexes: the Salzach-Enns fault zone in the Eastern Alps, Austria. *Journal of Structural Geologie, 20*, 799–818.

Weber, L., & Weiss, A. (1983). Bergbaugeschichte und Geologie der österreichischen Braunkohlenvorkommen. *Archiv für Lagerstättenforschung der Geologischen Bundesanstalt, 4*, 1–317.

Wessely, G. (1988). Structure and development of the Vienna basin in Austria. In: L. H. Royden, F. Horváth (Eds.), *The Pannonian basin* (vol. 45, pp. 333–346). Tulsa: American Association of Petroleum Geologists Memoir.

Wijbrans, J. R., Pringle, M. S., Koopers, A. A. P., & Schveers, R. (1995). Argon geochronology of small samples using the Vulkaan argon laserprobe. *Proc. Koninklijke Academie Wetenschappen, 98*, 185–218.

Winkler, A. (1928). Über Studien in den inneralpinen Tertiärablagerungen und über deren Beziehungen zu den Augensteinfeldern der Nordalpen. *Österreichische Akademie der Wissenschaften Sitzungsberichte mathematisch-naturwissenschaftliche Klasse Abt. 1*, 137, 183–225.

Zeilinger, G., Kuhlemann, J., Reinecker, J., Kázmer, M., & Frisch, W. (1999). Das Tamsweger Tertiär im Lungau (Österreich): Fazies und Deformation eines intramontanen Beckens. *Neues Jahrbuch für Geologie und Paläontologie Abhandlungen, 214*, 537–569.